Second harmonic generation from ZnO films and nanostructures.

Maria Cristina Larciprete, Marco Centini

Dipartimento di Scienze di Base ed Appzlicate per l'Ingegneria, Sapienza Università di Roma. Via Antonio Scarpa 14, 00161 Roma, Italy

ABSTRACT

Zinc oxide ZnO is a n-type semiconductor having a wide direct band gap of 3.37 eV along with an exciton binding energy of 60 meV at room temperatures which is considerably larger than ZnSe (22meV) and GaN (25 meV). The strong exciton binding energy of ZnO compared to the thermal energy at room temperature (26 meV), ensures an efficient exciton emission under low excitation energy.

The most thermodynamically stable phase of ZnO is the hexagonal wurtzite crystal structure, 6mm point group, where each Zn ion is surrounded by a tetrahedral of four O ions and vice versa. This tetrahedral organization results in a non-centrosymmetric crystal structure, allowing for second harmonic generation processes. For these reasons ZnO is a promising material for efficient second order nonlinear optical applications. Moreover, ZnO films and nanostructures can be easily prepared by a large variety of deposition techniques, thus being particularly attractive, for possible applications in integrated nonlinear optical devices. A lot of efforts have been spent to investigate how different efficiencies and properties of nonlinear optical processes, such as second (and third) harmonic generation, emerges from different deposition techniques and conditions.

In this review we present an extensive analysis of the main results obtained in the last years. The literature survey on ZnO films will include some significant features affecting second harmonic generation efficiency, as crystalline structure, film thickness, surface contributes and doping. In a separate section, the most prominent challenges in harmonic generation from ZnO nanostructures, are discussed, including ZnO nanowires, nanorods and nanocrystals, to name a few. Finally, the

conclusion part summarizes the current standing of published values for the nonlinear optical coefficients, for ZnO films and nanostructures, respectively.

I. INTRODUCTION

Second harmonic generation (SHG) has been the most investigated nonlinear optical process, since its discovery by Franken in the 1960's [1]. In frequency doubling processes, an incoming beam at frequency ω interacts with the nonlinear medium and, as a result, a second harmonic field (at frequency 2ω) is generated. This interaction is formally described by introducing a second order optical susceptibility of the nonlinear material, $\chi_{ijk}^{(2)}(-2\omega,\omega,\omega)$. Following a microscopic approach, two photons with the same energy interact with the nonlinear material and combine to generate a new photon with twice the energy, therefore half the wavelength, of the initial ones. Similarly the third harmonic generation (THG) process is responsible for the frequency tripling of the incoming beam by means of the third order susceptibility, $\chi_{ijkl}^{(3)}(-3\omega,\omega,\omega,\omega)$ which is a fourth rank tensor. While the THG, being an odd-order nonlinear optical process, it is symmetry-allowed in all materials, the SHG is an even-order effect, thus it is only allowed in those media lacking inversion symmetry. In other words, assuming the electric-dipole approximation, the third rank tensor components $\chi_{ijk}^{(2)}$, or equivalently the $\tilde{d}$ tensor terms, $d_{ijk} = \frac{1}{2}\chi_{ijk}^{(2)}$, presents non-vanishing terms only in those materials without centrosymmetric crystal structure. Materials belonging to a group symmetry without centre of inversion, give rise to so-called *bulk* or *electric dipole induced* SHG.

Beyond the bulk, electric-dipole contribution, arising from the non-zero terms of the nonlinear optical tensor, scientists agree that a significant contribution to the SHG signal from thin films and nanostructures maybe generated at grain boundaries and interfaces as well as from defects. These contributes can determine strong enhancement of the nonlinear susceptibility with respect to the bulk values, which may be experienced in very thin films. More significantly, second harmonic signal can also be generated from the surface, that itself represents a symmetry break. Thus, the structure of the nonlinear susceptibility tensor, $\chi_{ijk}^{(2)}$, may include further tensor elements that can be typically associated to surface effects. The different components of the third rank tensor $\chi_{ijk}^{(2)}$of a given

nonlinear optical material can be determined with reference to a well characterized sample, which is usually *α*-quartz, KDP or BBO, using several nonlinear optical techniques [2-3].

Concerning ZnO, its most thermodynamically stable phase is the wurtzite crystal structure, where each Zn ion is surrounded by a tetrahedral of four O ions and vice versa giving rise to a hexagonal primary cell. This tetrahedral organization results in a non-centrosymmetric crystal structure, *6mm* point group. For this reason, and for its wide transparency band in the visible range, ZnO is a promising material for efficient second order nonlinear optical applications. In this review paper we present a survey of the current status of SHG measurements from ZnO films and nanostructures. Following this brief introduction, section II describes the theory of SHG, with particular attention to ZnO crystalline lattice and its nonlinear optical tensor. Section III is devoted to the current status of SHG experiments from ZnO thin films. The effects of different issues as crystalline structure, thickness, surface contributions and doping on the nonlinear response is separately addressed in sub-sections. The main features of SHG from several ZnO nanostructures are reported in Section IV, including the main contributions related to third and higher order effects (i.e. THG and multi-photon luminescence) affecting the overall nonlinear optical response. For the sake of completeness, the most relevant works regarding THG from ZnO films are presented in Section V. Finally, Section VI concludes the review with an overview of the current standing of reported values for the nonlinear optical coefficients, that spread over by more than one order of magnitude.

II. SECOND HARMONIC GENERATION

The *c*-axis ZnO (0002) is grown with the hexagonal cell-axis perpendicular to the substrate surface. It presents five nonvanishing second order susceptibility tensor elements $\chi_{113}^{(2)}=\chi_{131}^{(2)}$; $\chi_{223}^{(2)}=\chi_{232}^{(2)}$; $\chi_{311}^{(2)}$; $\chi_{322}^{(2)}$ and $\chi_{333}^{(2)}$ [4]. The values of the nonlinear optical coefficients are typically measured in pm/V and, as a general rule, they depend on the incoming frequency via a dispersion relation. An abbreviated notation, the piezoelectric contraction, is usually adopted to replace the last

two subscripts of $\chi_{ijk}^{(2)}$ by a single subscript running from 1 to 6 (xx=1, yy=2, zz=3, yz=zy=4, xz=zx=5, xy=yx=6). The non-zero $\chi_{ijk}^{(2)}$ tensor elements become $\chi_{15}^{(2)}$; $\chi_{24}^{(2)}$; $\chi_{31}^{(2)}$; $\chi_{32}^{(2)}$ and $\chi_{33}^{(2)}$, or equivalently d_{15} ; d_{24} ; d_{31} ; d_{32} and d_{33}. Furthermore, the point group symmetry 6*mm* is invariant for rotation about the z-axis, thus the number of independent non vanishing coefficients reduce to three, being $d_{15} = d_{24}$; $d_{31} = d_{32}$ and d_{33}. Given all these considerations, the tensor $\tilde{d}$ can be written as:

$$\tilde{d} = \begin{pmatrix} 0 & 0 & 0 & 0 & d_{15} & 0 \\ 0 & 0 & 0 & d_{24} & 0 & 0 \\ d_{31} & d_{32} & d_{33} & 0 & 0 & 0 \end{pmatrix} = \begin{pmatrix} 0 & 0 & 0 & 0 & d_{15} & 0 \\ 0 & 0 & 0 & d_{15} & 0 & 0 \\ d_{31} & d_{31} & d_{33} & 0 & 0 & 0 \end{pmatrix} \quad (1)$$

The ideal wurtzite crystalline structure, in fact, retains additional internal relations between structural parameters. Indeed, far from absorption resonances, the crystal Kleinman's symmetry rules [5] further reduce the number of independent components. To a first approximation, the assumption $d_{31} = d_{15}$ and $|d_{33}| = 2d_{31}$ is allowed. As a consequence, under specific circumstances, it is possible to limit the investigation only to the measurement of the largest component, i.e. d_{33} [6-7]. Alternatively, near the band gap it is necessary to characterize the different nonlinear optical tensor elements independently. In this situation, the components of the second order susceptibility can be addressed by choosing different polarization states for fundamental and generated beam, respectively. Furthermore, the spectral investigation over the same film structures reveal that nonlinear optical susceptibiliy considerably increases as the SH frequency approaches the material bandgap.

Several experimental methods have been developed, for the determination of values (and signs) of all nonzero components of the nonlinear susceptibility tensor in crystals. Since its introduction, the Maker fringes technique [8], which is based on the investigation of oscillations of the SH intensity by changing the crystal thickness, has been one of the most used.

Briefly, this technique consists in measuring the SH signal transmitted through the crystal as a function of the incidence angle of the fundamental beam, which can be varied by placing the sample

onto a rotation stage. The polarization states of fundamental and generated beams are selected by rotating a half-wave plate (polarizer) and a linear polarizer (analyzer), placed before and after the sample, respectively. In order to minimize the influence of laser energy fluctuations, a fraction of the fundamental beam is split to a reference line of the setup, where the SH signal from a well characterized reference crystal, for example a quartz plate, is simultaneously measured at a fixed incidence angle.

The full expression of the SH power $W_{2\omega}$, as a function of the incidence angle, α, including the effect of absorption, trough the extinction coefficient at the fundamental, k_{ω}, and at the second harmonic frequency, $k_{2\omega}$, can be written as [9-10]:

$$W_{2\omega}(\alpha)=\left(\frac{512\pi^3}{A}\right)\cdot t^4{}_{\omega}(\alpha)\cdot T_{2\omega}(\alpha)\cdot W_{\omega}^2\cdot\frac{\sin^2(\Psi(\alpha))+\sinh^2\left(\chi^{HH}(\alpha)\right)}{(\Psi(\alpha))^2+\left(\chi^{HH}(\alpha)\right)^2}\left(\frac{\pi L}{\lambda}\right)^2\cdot d^2{}_{eff}(\alpha) \tag{2}$$

where A is the fundamental beam transverse area as projected onto sample surface and retrieved from the pump beam area (A') as $A=A'/\cos(\alpha)$), t_{ω} is the Fresnel transmission coefficient for the fundamental field at the input interface, $T_{2\omega}$ is the Fresnel transmission coefficient for the SH power at the output interface, and L is sample thickness.

The power, P_{ω}, of the incident fundamental beam is taken into account in the term $W_{\omega}^2=P_{\omega}^2\cdot e^{-2\delta}$, which also includes an attenuation factor given by:

$$2\delta=\left(\frac{\pi L}{2}\right)\frac{4}{\lambda}\left(k_{\omega}\cos(\alpha'_{\omega})+k_{2\omega}\cos(\alpha'_{2\omega})\right) \tag{3}$$

where α'_{ω} and $\alpha'_{2\omega}$ are the internal refraction angles corresponding to fundamental and generated beams.

The phase factor $\Psi(\alpha)$ takes into account material dispersion through n_ω and $n_{2\omega}$, the refractive indices at the fundamental and generated frequency, respectively:

$$\Psi(\alpha) = \left(\frac{\pi L}{2}\right) \cdot \left(\frac{4}{\lambda}\right) \cdot \left(n_\omega(\alpha) \cdot \cos(\alpha'_\omega) - n_{2\omega}(\alpha) \cdot \cos(\alpha'_{2\omega})\right) \tag{4}$$

Due to materials' anisotropy, $n_\omega(\alpha)$ and $n_{2\omega}(\alpha)$ may depend on the polarization angles of fundamental and generated beams as well as on incidence angle.

The term $\chi^{\mathrm{HH}}(\alpha)$ introduced by Herman and Hayden is an additional phase term which takes into account the effect of losses on the Maker fringes, arising if the imaginary part of the refractive index is non-zero. Likewise the material absorption reduces the amplitude of the wave, the shape of the angular curve itself is modified by [11]:

$$\chi^{\mathrm{HH}}(\alpha) = \left(\frac{\pi L}{2}\right)\left(\frac{4}{\lambda}\right)\left(k_\omega \cdot \cos(\alpha'_\omega) - k_{2\omega} \cdot \cos(\alpha'_{2\omega})\right) \tag{5}$$

Finally, the term $d_{\mathrm{eff}}(\alpha)$ in Equation (2) holds for the *effective* optical nonlinearity, arising from the second order nonlinear optical tensor. The general expression for $d_{\mathrm{eff}}(\alpha)$ is rather complicated being dependent on the polarization state of both first and second harmonic electric fields respectively and, of course, on the fundamental beam incidence angle, α. However, it can be significantly simplified for particular crystalline symmetries. In what follows, we will use indifferently $\chi_{ij}^{(2)}$ or $d_{ijk} = \frac{1}{2}\chi_{ijk}^{(2)}$ to mention the nonlinear optical coefficients.

In general, the polarization angle, ϕ, is defined with respect to the incidence plane and may assume all possible values ranging between 0° (*p* polarization) and 90° degrees (*s* polarization). This implies that for the *p*-polarized wave the electric field oscillates within the plane of incidence, while

for *s*-polarization the oscillation direction is perpendicular to the plane of incidence. Changing the polarization state of both fundamental and generated beams, different nonlinear optical tensor components can be separately address. Considering the ZnO group symmetry, the final expressions for $d_{\mathrm{eff}}(\alpha)$ for three significant polarization configurations are:

$$
\begin{aligned}
d_{eff}^{s_\omega p_{2\omega}} &= d_{31}\sin\alpha_{2\omega} \\
d_{eff}^{45_\omega p_{2\omega}} &= d_{15}\sin\alpha_{\omega} \\
d_{eff}^{p_\omega p_{2\omega}} &= d_{15}\cos\alpha_{2\omega}\sin 2\alpha_{\omega} + d_{31}\cos^2\alpha_{\omega}\sin\alpha_{2\omega} + d_{33}\sin^2\alpha_{\omega}\sin\alpha_{2\omega}
\end{aligned}
\qquad (6)
$$

where the apices s_ω-$p_{2\omega}$, 45_ω-$p_{2\omega}$ and p_ω-$p_{2\omega}$ refer to three different polarization combinations of fundamental and generated beams, respectively. Equations (6) show that, from the experimental point of view, the term d_{31} can be independently evaluated from the measurement of the *p*-polarized SH signal for a *s*-polarized fundamental beam; d_{15} can be retrieved from data corresponding to *p*-polarized SH signal for a *45*°-linearly polarized fundamental beam. Finally, the largest component, d_{33}, is addressed when both SH and fundamental beams are *p*-polarized. The expression of d_{eff} in the latter case also includes a dependence on d_{31} and d_{15} which should be determined separately. Nevertheless, if Kleinman's symmetry rules apply, by fitting only the p_ω-$p_{2\omega}$ measurements, which also result in the strongest SH signal, one may directly retrieve the value of d_{33}. Some authors therefore limited their investigation to the measurements of the largest component, i.e. d_{33}.

On the other hand, whenever Kleinman's symmetry is broken and the ratio d_{33}/d_{31} can significantly deviate from the ideal value, an independent evaluation of the three components, or at least two of them, is more appropriate.

Typical Maker fringe patterns measured from a ZnO film, some hundreds of nm thick, are shown in Figure 1(b). The angularly resolved SHG signals arising from the *c*-axis oriented ZnO films go to zero at normal incidence for both *p*-polarized and *s*-polarized fundamental beam. As evidenced

from the experimental curves, *p* polarization of the fundamental beam generally produces higher SH signals.

Alternatively to Maker fringes experimental configuration, the reflective second harmonic generation (RSHG) scheme involves the detection of theSH signal in reflection mode, at a fixed incidence angle, as a function of the azimuthal angle θ, which is the angle between the incidence plane and the *x*-axis on the sample surface, as shown in Figure 2(a). Briefly, in this experimental configuration the sample is rotated along its surface normal, i.e. along the *z*-axis, while the reflected SH signal is systematically measured.

The *p*-polarized [12] and *s*-polarized [13] SH signals originating from the group symmetry 6*mm* as a function of the azimuthal angle θ are respectively given by:

$$\begin{aligned} P_{bulk}^{p\omega p2\omega} &= d_{15}E_0^2\hat{x} + \frac{1}{2}(d_{31}+d_{33})E_0^2\hat{z} \\ P_{bulk}^{s\omega p2\omega} &= d_{31}E_0^2\hat{z} \\ P_{bulk}^{p\omega s2\omega} &= 0 \\ P_{bulk}^{s\omega s2\omega} &= 0 \end{aligned} \tag{7}$$

First of all, Equations (7) rule out the dependence of *p*-polarized SH signal on the azimuthal angle, if the direction of ZnO (0002) is the z-axis of the film. As a consequence, the p_ω-$p_{2\omega}$ SH curves are centred on the polar (radar) diagram, as shown in Figure 2(b) [12]. Eventually, a tilt of the ZnO (0002) direction may cause an asymmetric shift of the resulting SH curve from the centre of the polar diagram.

More interestingly, the nonlinear susceptibility tensor for the group symmetry 6*mm* does not allow bulk electric dipole contribute to the RSHG in the s_ω-$s_{2\omega}$ configuration [13]. Beyond bulk SHG, it was found that the second harmonic signal can be generated also from a bare surface, that itself corresponds to a symmetry break in space [14]. Being the total generated SH signal composed by both

bulk and surface contributions, it is thus possible to isolate only surface related SH signal via RSHG technique, when both the fundamental and generated beams are *s*-polarized. In fact, the occurrence of a non-zero signal in the $s_{\omega} s_{2\omega}$ configuration is used to probe the non-vanishing polarity induced by surface effects.

Beside single pump beam configurations, also two separate pump beams have been employed to observe SHG from thin ZnO films, either at the same frequency [15-16] or having different frequencies [17]. In general, the interaction of two pump beams linearly polarized, tuned at ω (or at ω_1 and ω_2) with a noncentrosymmetric material, produces a nonlinear polarization oscillating at the frequency 2ω (or $\omega_1+\omega_2$). In the first experimental configuration [18], the two-beams are employed to investigate SHG from ion beam sputtered ZnO films. The fundamental beam is split into two beams of comparable power, while the temporal overlap of the incident pulses is controlled with an external delay line, and both beams are sent to intersect onto the sample surface, with two different incidence angles. According to the wave vectors' conservation law, the generated beam is emitted nearly along the bisector of the aperture angle between the two pump beams. Varying the polarization state of both fundamental beams it is possible to obtain a map of the SH signal as a function of the polarization states of both pump beams, which is characteristic for any different symmetry structure. The investigation of this polarization map allows to retrieve the values of the nonlinear optical coefficients and it is also an useful tool to control the orientation of the optical axis and its angular tilt, with respect to the surface normal [15]. Moreover, coherent bicolour interaction was employed to show that the second order susceptibilities of ZnO nanocrystallite films can be enhanced using Au nanoparticles [17]. The pump beam consists of a superposition of the fundamental and the doubled frequency wavelength of a ps Nd:YAG laser. The ratio of their intensities is changed by varying the polarizations of fundamental and doubled frequency beams, while the second beam is responsible for forming a nonlinear optical grating onto the ZnO film, which further enhance the SH signal.

III. SHG IN ZNO THIN FILMS

Nonlinear optical response from thin films is particularly attractive, since thin films can be easily integrated in nonlinear optical devices. For what concerns ZnO films, the large variety of preparation methods, as well as the different possible contributions to SHG signal, are responsible for the wide spread of reported experimental values for the nonlinear optical coefficients, that may differ by more than one order of magnitude.

Second order nonlinear optical response has been experimentally demonstrated from ZnO films grown by pulsed laser ablation [19], spray pyrolysis [20-21], laser deposition [22], reactive sputtering [23] as well as self-assembling by Laser-MBE [24-25], metalorganic chemical vapour deposition [26], dual ion beam sputtering [27-28], rf magnetron sputtering [29-32], metal organic aerosol deposition [33], gas transport reaction technique [34], plasma assisted molecular beam epitaxy [35]. Furthermore, a reduced number of works report on third harmonic generation from ZnO nanocrystalline films [28, 30, 36-40].

Typically, thin films are grown in a polycrystalline state which is characterized by a distribution of grains, i.e. spatial domains having the same crystal orientation. In some cases the orientation distribution within the grains results in a mean direction of the optical axis, thus affecting the nonlinear optical tensor components. The size of the grains also plays an important role because part of the SH signal is produced at grain boundaries or by defects such as stacking faults. These circumstances are not always easily predictable and are strongly dependent on the growing method likewise on the type of substrate.

Conversely, following these considerations, second harmonic measurements represent a useful tool to indirectly assess the crystalline quality of a given thin film. Besides nonlinear optical characterization, other complementary methods, as for instance the x-ray diffraction (XRD) patterns, scanning electron microscopy (SEM) or atomic force microscopy (AFM), allow to characterize the distribution of the grain size. By comparison with other conventional characterization methods, in fact, nonlinear optical measurements can also be employed as a suitable and sensitive method for testing the textures of ZnO films fabricated by different techniques and conditions of growth [13].

As well as for the linear optical susceptibility, the second order susceptibility is also subject to the effect of dispersion, i.e. the values of the nonlinear optical coefficients are frequency-dependent, thus a more comprehensive investigation should include the wavelength dependence of the second order susceptibility. For instance, in Reference 28 SHG measurements were carried out by means of the rotational Maker fringes technique in the transmission scheme and the dispersion of the second order nonlinear optical tensor for ZnO films grown by dual ion beam sputtering has been investigated for three different fundamental wavelengths, i.e., 1064 nm, 1542 nm and 1907 nm.

In order to address the potential of a particular deposition technique, it's worth to investigate how the methodical change of a given parameter during film growth may affect the resulting nonlinear optical properties. So for instance, with reference to magnetron sputtering technique, the effect of substrate temperature was studied and it was shown [13, 29] that the second harmonic signal measured in reflection decreases as the temperature of the substrate during deposition increases. Concerning ZnO films grown by dual ion beam sputtering (DIBS), the influence of the oxygen content in the deposition chamber over the second order nonlinear optical properties has been investigated [27]. Finally, the effect of varying rf power on the resulting SHG from ZnO films deposited by rf sputtering was also addressed [32].

In addition to the different deposition techniques, also a large variety of materials was successfully employed as substrates. The most commonly used are sapphire [23-26, 33-35] and glass [20-21, 23, 27-28], since they do not give bulk contribute to the second harmonic signal. The possibility, explored in some works, to get second order nonlinear optical response from ZnO films grown on silicon substrate is particularly attractive since it is expected to offer the further advantage to integrate ZnO with the Si-based microelectronics devices [13, 29, 31-32]. Finally, considering the employ of crystals substrates, as for instance quartz [40], α-BBO or $LiNbO_3$ [30], it must be pointed out that the use of noncentrosymmetric structures has to be carefully checked because they may also produce spurious contribute to SH signal and, therefore, can significantly influence the SHG measurements.

In practically all the works presented up till now, ZnO films with the crystallites axis oriented about perpendicular to the substrate surface are employed. One has to ascribe the reason for that to ZnO hexagonal lattice, which shows a strong tendency to crystallise with such orientation, and so-called *c*-axis oriented films can be easily produced on polycrystalline or amorphous substrates by different techniques. As a consequence, very seldom ZnO films with *a*-axis orientation (11$\underline{2}$0) have been investigated for SHG, i.e. films where the crystallites axis is aligned parallel, rather than normal to the substrate surface. When grown with this particular orientation, the ZnO films display peculiar Maker fringes patterns, with respect to *c*-axis oriented films, as shown in Figure 3. First of all, a maximum in the SH signal appear just at normal incidence, i.e. where it is forbidden for *c*-axis oriented films. Furthermore, the total conversion efficiency in *a*-axis ZnO is strongly increased with respect to *c*-axis ZnO [33].

Given the large amount of experimental works by different authors, which are summarized in Table I, SHG has been correlated to several structural factors such as crystalline structure [19, 21, 24], including grain size and shape [21] and crystallites' orientation [33], film thickness [21, 23, 25] or the introduction of dopant elements [21]. The effect of different factors affecting SHG from ZnO films will be discussed in the following sub-sections.

A. THE EFFECT OF CRYSTALLINE STRUCTURE

In polycrystalline films both electronic and optical properties, including second harmonic generation, can be affected by the structure of grain boundaries. Grain boundaries, as well as defects, represent a break in the crystalline structure, i.e.a break in the symmetry that itself can be a source of SHG. Furthermore, as the crystalline order in different neighbouring grains slightly change orientation, it is likely that grains themselves represent a way to increase SHG.

Regarding SHG from ZnO films, the effect of grain boundaries emerged from the experimental evidence that film with lower crystallinity may show larger second order nonlinear optical response, with respect to film with higher crystallinity. This effect was observed for the first time by Cao et al.

[19] in both thin (45 nm) and thick (235 nm) ZnO films deposited by pulsed laser ablation. SH measurements in the Maker fringes configuration were performed from two couples of films having same thickness but different crystallinity (verified by XRD), and the absolute values of the nonlinear optical coefficients were retrieved. The experimental SH curves, together with the XRD results show that samples with lower crystallinity exhibit more efficient SH signals, thus confirming that the SH signal is generated not only in the crystallites (bulk) but also at grain boundaries. Furthermore, it was found that the thicker films have lower nonlinear optical coefficients thus authors infer that part of the SH signal arises from interfaces.

The experimental results obtained in this work represented the beginning of a deeper, more comprehensive investigation of the mechanism of SHG from polycrystalline ZnO films.

In order to put in evidence a correlation between SH efficiency and the grain size in ZnO films, Neuman et al. [21] systematically probed a large set of 70 specimens, ranging from 0.1 to 1 μm in thickness, prepared by spray pyrolysis technique. SHG was investigated as a function of both thickness and grain size, by using the Maker fringes scheme. At the same time, SEM images allowed to perform the grain size statistics of sample surfaces. Nevertheless, despite the high number of samples investigated in this accurate work, neither a clear dependence on thickness nor a direct correlation with grain size emerged from experimental results. Thus, in order to take into account crystallites shape and size, a parameter called the normalized surface ratio (σ) was introduced. The ZnO crystallites were treated as columns of height h and square cross section d_i^2. This new structural parameter takes into account the columns height as well as the aspect ratio of the ZnO such crystallite columns:

$$\sigma = \sum_i \left(2d_i^2 + 4d_i h\right) \Big/ \sum_i d_i^2 \tag{8}$$

Investigated samples were classified using σ, as shown in Figure 4. By authors' admission, the prevalence of a particular aspect ratio, coming out from experimental data, can be merely the result of

a coincidence of growth parameters causing both a particular aspect ratio and efficient SHG. More significantly, the structure of the nonlinear susceptibility tensor, $\chi^{(2)}$, which was reconstructed from the angular dependence of SH signals, does not include new tensor elements that can be typically associated to surface effects. Thus, from experimental evidences, authors observed that films showed even more efficient second harmonic generation than the bulk crystal, indicating grain boundaries and interfaces effects. A correspondence between the grain structure and SHG efficiency is finally recognized, and still bulk effects, including grain boundaries effects, dominate the SH intensity in a few hundreds of nm thick films [21].

The effects of grain boundaries on SHG are studied also in Ref 12, where the influence of substrate temperature (100-300 °C) on the film structural and nonlinear optical properties is investigated. Indeed, among the different possible growth conditions, temperature is one of the most important parameters that determine the quality of epitaxial films and thus it also affects the resulting SHG. Several ZnO films, 1.06 μm thick, with *c*-axis orientation were grown by RF magnetron sputtering on Si(111) substrate. In addition to reflective second harmonic generation (RSHG), X-ray diffraction and scanning electron microscopy (SEM) have been used to analyze the quality of the crystallite structure. The experimental curves obtained for the p_{ω}-$p_{2\omega}$ signal via 360° azimuthal scanning, show that the RSHG signal intensity from ZnO films, corresponding to the curve radius (Figure 2b), decreases as substrate temperature is increased. On the other hand, the SEM images indicate that the grain size increases with increasing substrate temperature. Comparing the experimental results with the characteristic grain size parameters, the correlation between the RSHG intensity and the substrate temperature reveals that the effect of the grain boundaries is the dominant part of the RSHG mechanism.

In the work of Liu et al. [26], several ZnO films, 350 nm thick, grown by metallorganic chemical vapour deposition (MOCVD) on sapphire substrates were investigated. The SHG was measured in the Maker fringes configuration [8-9] from films deposited at different temperature, ranging from 200 to 500 °C. Once more, the experimental investigation associates the strongest SHG

intensity to the samples with lowest crystalline quality, occurring at deposition temperature of 250 °C. This enhancement is ascribed both to the poor crystallinity and to film defects. The explanation of experimental results in terms of film defects given in Reference 26 is the following: in the ideal conditions, the unit cells possess the same in-plane orientations within the whole film, and one unit cell is connected with the neighbouring by similar atomic bounds, i.e. these bounds are in their ‘‘equilibrium’’ positions. When the in-plane orientations of two adjacent unit cells are different, as in the real films, the atomic bounds among them will deviate from their equilibrium positions. This may favour the formation of dangling bonds at the interfaces of different unit cells, which in turn results in extra carriers or film defects. In fact, it has been demonstrated that an increasing in carrier density and defects can enhance [41] the optical nonlinearity in crystals.

Another deposition parameter affecting the quality of the resulting film is the oxygen pressure applied during film growth. Nanocrystalline laser deposited ZnO thin films grown at different oxygen pressure (100 and 900 mTorr, respectively) were investigated [39], and both SH efficiency and TH efficiency were found to be correlated to the resulting crystallites' size. In particular, the smaller particle size (8 nm) film, grown with the lower oxygen pressure, was associated to the higher $\chi^{(2)}_{eff}$=3.2 pm/V and $\chi^{(3)}$=9.56·10^{-12} esu. On the other hand, the bigger particle size (84 nm) film, resulting from high oxygen pressure deposition, provided $\chi^{(2)}_{eff}$ =0.7 pm/V and $\chi^{(3)}$=1.2·10^{-13} esu.

The use of different substrates also affects the crystalline structures. In Reference 30, for instance, ZnO thin films were deposited by RF magnetron sputtering on two different crystals, α-BBO (0012) and $LiNbO_3$ (0001), respectively. While XRD patterns reveal that the grain size of the ZnO film is not dependent on the type of substrate, linear transmittance spectra indicate that the film deposited on lithium niobate possesses better structural quality and higher degree of crystallinity. The SHG measurements, performed in the Maker fringes scheme, provide for the effective values of the nonlinear optical coefficients, $\chi_{eff}^{(2)}$, extremely different values for the two types of substrate. The low value obtained for the α-BBO substrate, $\chi_{eff}^{(2)}$ =0.23 pm/V, is entirely ascribed to the ZnO film, being the α-BBO a centrosymmetric crystal. The much higher value obtained for the $LiNbO_3$ substrate, $\chi_{eff}^{(2)}$

= 12.9 pm/V, is ascribed to the little lattice misfit between ZnO and $LiNbO_3$ (-8.44%) which is even lower than for ZnO/Sapphire (-15.53%) [42]. However, it must be pointed out that the Maker fringes curve presented [30] for the latter case may possibly include a contribute from the $LiNbO_3$ substrate [43], which is a good nonlinear material and may itself significantly contribute to the SHG.

The role of a high density of crystalline grains is also addressed in Ref.34, where a ZnO film 110 nm thick was fabricated on (0001) sapphire substrate by the modified chemical vapour deposition method and its SHG response was investigated. The SH signal is measured as a function of the sample rotation azimuthal angle and the ratios of the nonlinear optical components $r_1=d_{31}/d_{33}$ (or d_{32}/d_{33}) and $r_2=d_{24}/d_{33}$ (or d_{15}/d_{33}) are retrieved. The theoretical model adopted in [34] allows to indirectly evaluate the enhancement of the components d_{33} and d_{31} in the film with respect to the single crystal, thus confirming the significant contribute of grain boundaries on SHG efficiency.

So far, these examples show that, beyond the bulk, electric-dipole contribution, arising from the non-zero terms of the nonlinear optical tensor, a significant part of the SHG signal from thin films may be generated at grain boundaries and interfaces. Given this consideration, most authors agree that decreasing both grains size and crystallinity degree, leads to enhanced SH signal. These contributes give explanation for the strong enhancement of the overall nonlinear susceptibility, experienced in some cases, for very thin films with respect to the bulk values. All the mentioned results, in terms of nonlinear optical tensor values, are summarized in Table II.

B. THE EFFECT OF THICKNESS

Experimental evidences show that film thickness may significantly affect the second-order susceptibilities. Many systematic studies, in fact, were performed in order to highlight the dependence of second harmonic efficiency on film thickness.

An extensive study [23] on films whose thickness ranged between 5 and 350 nm was performed by Wang et al. Films were prepared by two different methods, i.e. reactive sputtering and plasma enhanced chemical vapour deposition. Under Kleinman's approximation (i.e. $\chi_{15}^{(2)}=\chi_{24}^{(2)}$

$=\chi_{31}^{(2)}=\chi_{32}^{(2)}= 0.5\ \chi_{33}^{(2)}$), it was found that the absolute values of the nonlinear optical components decrease with the film thickness, while the ratios between the two non-zero components $\chi_{31}^{(2)}/\chi_{33}^{(2)}$ show no evidence of a dependence on the film thickness. As reported in Table III, for thinner films, the nonlinear optical coefficient can be as large as $\chi_{33}^{(2)}= 17.89$ pm/V (for the 44.2 nm thick film) while it drops to $\chi_{33}^{(2)} = 7.80$ pm/V for the 343.5 nm thick film. In Figure 5 the $\chi_{33}^{(2)}$ values are reported as a function of different film thicknesses [23]. The second-order susceptibilities decrease is interpreted according to a model in which the *c*-axis, which is supposed to be initially aligned with respect to the substrate normal, flips when the film thickness increases, thus deteriorating the nonlinear optical response.

A peculiar peak-like effect, in thickness, was observed in Ref [25] where several ZnO films grown by laser molecular beam epitaxy (at 500°C) ranging from tenths to hundreds of nm were investigated. The SH signal, measured at a fixed polarization angle, as a function of the fundamental beam polarization angle, allowed the recovery of the nonvanishing components of the nonlinear optical tensor. In particular, an extraordinary enhancement of the optical nonlinearity is reported for a sample 44.4 nm thick (see Table III), whose nonlinear optical components dramatically peak to $d_{33}= -83.7$ pm/V, $d_{31}= 14.7$ pm/V and $d_{15}= 15.2$ pm/V, exceeding by nearly 14 times those of bulk ZnO [25]. Outside the enhancement range, 35-65 nm in thickness, the susceptibilities are small and almost the same as those for bulk material. The observed enhancement is explained considering the microcrystallite characteristics obtained via atomic force microscopy (AFM), scanning tunnelling microscopy (STM) and transmission electron microscopy (TEM). A thin film with a thickness within 35 and 70 nm consists of hexagonal-shaped columns with lateral nanocrystals sizing from 40 to 60 nm separated by grain boundaries perpendicular to the *c*-axis. As the film thickness increases, the crystallinity of the film increases as well, possibly leading to the increase of the bulk second-order non-linear effect. However, the average grain size is also increased together with the film thickness [44], thus reducing the grain boundaries contribution to SHG. These two contrasting tendencies end up

with a peak-like structure of the second-order non-linear susceptibilities vs thickness, and give an explanation to the experimental results.

The mentioned works witness the efforts in finding a correlation between thickness and second harmonic efficiency in ZnO films. Nevertheless, authors agree that a clearcut dependence is yet to be found, mostly because thickness is not the unique factor affecting SH efficiency.

C. SURFACE CONTRIBUTES

Thought it was believed that crystals could only exhibit second harmonic generation if the crystal lacks of centro-symmetry, second harmonic generation from a surface was experimentally observed for the first time by Terhune and co-workers, from a centrosymmetric crystal of calcite [45]. In 1968, Bloembergen et al. [14] pointed out that SH signal can be generated from a surface, that itself represents a symmetry break. Later on it was shown that surface SHG could be employed for single monolayer detection [46] and since then, surface SHG was developed as a detection method of molecular adsorption and orientation.

From the point of view of SHG process, an interface represents an extremely interesting issue. At a crystalline surface half of the atomic forces experienced inside the bulk crystal vanishes, thus causing deviations in the atomic and electronic structures. The main consequences occurring at interfaces is the variation of interplanar distances of the top layers as well as the redistribution of the atoms to a different packing structure. Even if symmetry is maintained within the surface planes, the out-of-plane break in symmetry modifies the second-order susceptibility tensor $\chi^{(2)}$, giving rise to novel non-zero coefficients.

Typically, measurements of surface SHG are performed by rotating the sample with respect to the incident beam, i.e. about the z-axis (see Figure 2(a)). The RSHG signal varies with the azimuth angle of the sample due to the symmetry of the atomic and electronic lattice.

Moreover, in addition to surface terms, thin films and bulk crystals may contain a high density of extended defects, such as stacking faults, dislocations, symmetrical tilt grain boundaries and twin

boundaries. These extended defects naturally occur in ZnO thin films due to the lattice mismatch between film itself and the substrate. Furthermore, also the discrepancy between the thermal expansion coefficients may play a role in the process of defects formation.

For ZnO films, particular attention has been given to the formation of twin boundaries defects [31-32]. By definition, twin boundaries stands for the regular growing together of crystals of the same sort, so that only a slight misorientation exists between them. They spontaneously occur during crystal growth or can be induced through mechanical stress. So-called twinned crystals are two adjacent crystals sharing a single composition surface often appearing as mirror images across the boundary. As a consequence, the polarity in the twin boundary exhibits a mirror symmetry across the boundary plane [47], very frequently with one crystal being the mirror image of the other, giving rise to a source of nonlinear optical signal, if appropriately stimulated.

The effect of both the surface contribution, arising from the polar Zn–O bond on the top layer, and the additional contribution of twin boundaries was investigated from ZnO (0002) prepared by MOCVD on sapphire [13]. Surface related SHG was measured via reflective SHG (RSHG) using *s*-polarization for both fundamental and generated beams. This polarization configuration is particularly interesting because the bulk SHG signal resulting for 6*mm* symmetry is forbidden, thus the generated signal is a signature for other than bulk effects. In other words, when both fundamental and generated beams are polarized perpendicularly to the plane of incidence, the symmetry of the surface structure can be investigated.

On one side, at the film surface the polar Zn-O bonds break the bulk symmetry, i.e. the hexagonal close packed structure 6*mm* point group symmetry, and form a layer having *3m* symmetry on the well grown 6*mm* ZnO. On the other side, the formation of twin boundaries, induced by the lattice mismatch with the substrate is responsible for a non-vanishing polarity [47], which exhibits a mirror relation across the boundary plane. The resulting second-order nonlinear optical susceptibility tensor includes six independent components. The outcome is that the experimental s_{ω}-$s_{2\omega}$-RSHG

patterns evidence both the *3m*-like symmetry structure on the surface of ZnO (0002) and the additional twin boundaries contribution with mirror like symmetry.

Both the effect of twin boundaries and polar surface, are taken into account using the fitting equation introduced by the authors [13]:

$$I_{ss} = \left| ae^{i\psi} \sin(\phi) + b \sin(3\phi) \right|^2 \tag{9}$$

since parameter *a* represents the strength of nonlinearity due to the formation of twin boundaries and parameter *b* the polar strength of Zn–O bonding induced 3*m* symmetry, respectively. The relative phase difference between the SHG field from the 3*m* symmetric structure of Zn–O bonding and twin boundaries is represented by the term ψ. The resulting pattern of the RSHG azimuthal scanning is shown in Figure 6, where the peculiar six-fold profile reflects the simultaneous contributions of both the 3*m* group symmetry and twin boundaries.

The bare effect of twin boundaries was almost isolated [31] by investigating ZnO thin film grown on Si (111) substrate, whose surfaces were intentionally polished in order to eliminate the RSHG contribution of 3*m* symmetry [13]. Once more the RSHG measured in s_ω-$s_{2\omega}$ polarization configuration is employed to probe the nonvanishing polarity of twin boundaries in a ZnO film. The overall effect of the lone twin boundaries contribution on the strained interface corresponds to a mirror-like second order susceptibility tensor with the elements $\chi_{xxx}^{(2),m}$ and $\chi_{xyy}^{(2),m}$, where the *x* direction is parallel to the boundary plane and the *y* direction is perpendicular to the boundary plane. The modified second-order susceptibility leads to a nonvanishing $s_\omega s_{2\omega}$-RSHG intensity which can be expressed explicating the tensor elements [31]:

$$I_{ss} = \left| \cos\phi \left(\chi_{xxx}^{(2),m} \cos^2\phi + 2\chi_{xyy}^{(2),m} \sin^2\phi \right) \right|^2 \tag{10}$$

The mirror-like symmetrical RSHG azimuthal curves given by Equation (10) result in a two-lobed pattern, shown in Figure 7 in which there is no additional symmetrical contribution from the group symmetry 3*m*. Likewise, the experimental azimuthal scan, forms two-lobed symmetric patterns indicating that the grain boundaries have a polar configuration across the boundary plane and possess a directional arrangement [31].

A slight asymmetry that may appear in the two lobed pattern, in disagreement with Equation (10), would denote that the twin boundary does not have a mirror symmetry, i.e. the two planes shift one relatively to the other one along the twin boundary [47], due to a stress gradient. As a result, the mirror structure with forward-backward symmetry is broken. This effect can be taken into account by introducing the stress gradient with an empirical parameter *a* [31]:

$$I_{ss} = \left|\cos\phi\left(\chi_{xxx}^{(2),m}\cos^2\phi + 2\chi_{xyy}^{(2),m}\sin^2\phi\right) + a\right|^2 \tag{11}$$

Despite the efforts of several authors, the formation mechanism of twin boundaries as well as the relationship with the film quality under various film growth conditions is yet to be completely understood. In Reference 32, ZnO films were deposited on Si (111) substrates by RF sputtering and the RF power was systematically changed in the range 40-100 W, thus influencing the formation and ordering of ZnO grain boundaries. RSHG was then employed to analyze the symmetric structure of ZnO grains, whose net direction changes with RF power.

Experimental results [32] show that the value of $\chi_{xxx}^{(2),m}$ depends on the amount of symmetrical polar structures at the boundaries. It reaches a maximum in correspondence of a mimimum of FWHM X-ray diffraction (XRD) peak, which results in the best crystallinity among the investigated samples. If sputtered atoms have suitable migration energy and deposition time to form better quality ZnO film, more regular boundary planes are formed. On the other hand, the value of $\chi_{xyy}^{(2),m}$ is not affected by RF power. Furthermore, twin boundaries are preferentially formed along the (110) direction, i.e. under

the lowest energy condition [47]. Possible shift of the two lobed symmetry patterns would indicate a tilt angle with respect to the preferential direction. This angular shift can eventually be included in the theoretical fitting curve [32].

The effect of surface roughness on SHG was systematically studied on polarity-controlled ZnO films grown onto different buffer layers on (0001) sapphire substrates by plasma assisted molecular beam epitaxy [35]. Selective growths of Zn-polar and O-polar ZnO were achieved by introducing MgO and Cr compound buffer layers, respectively. At the end of these processes, four types of ZnO films were realized, two Zn-polar ZnO films (grown on 7-nm-thick MgO and CrN buffer layer), and, for comparison, two O-polar ZnO films (grown on 1.5-nm-thick MgO and Cr_2O_3 buffer layers) [35]. Film thickness ranged from 270 to 450 nm. The effective second-order NLO coefficient was determined by using the Maker fringes technique. The experimental results show a correlation between d_{eff} and the grain size and thus surface roughness. Specifically, it was found that the d_{eff} of the ZnO films increased with decrease in the grain size and surface roughness, as shown in Figure 8. This effect can be explained by the increase of surface scattering experienced by the fundamental beam as grain size and surface roughness are increased, respectively.

In conclusion, surface effects does not give significant enhancement of the second order susceptibility, but rather change its form. Thus, surface SHG represents an efficient tool to probe the dynamics of absorption (and desorption) of atomic and molecular species on ZnO thin films. As an example, time dependent SHG using a pump beam tuned at 740 nm was used to investigate the interaction between O_2 and ZnO surface defect sites [48]. Adsorption of O_2 on ZnO thin films, in fact, induce an electric field at the surface of ZnO leading to electric field induced SHG (EFISH). On the other hand, if the pump photon energy is enough to excite electrons across the band gap of ZnO, the pump beam itself forces the decay of the EFISH signal. The strong sensitivity of SHG to charges at semiconductor surfaces and interfaces is currently employed to investigate the kinetics of absorption/desorption of atomic and molecular species on thin films, in the seek of applications such as optical sensors.

D. DOPING

Doping, i.e. the intentional addition of impurities to a given material within the growth process, produces remarkable changes in the corresponding electrical, morphological, and optical properties. As a general rule, the effect of the dopant element depends on its electronegativity and ionic radius. For what concerns ZnO, it is experienced that doping with donor impurities to achieve high n-type conductivity is less difficult than doping with acceptor impurities to achieve p-type conductivity. Indeed ZnO is a naturally n-type semiconductor because of intrinsic defects such as oxygen vacancies [49].

Several reports on doping of ZnO thin films are available, such as doping with In [50–51], Ga [52] Li [53], F [54] although these works only deal with structural, electrical and/or linear optical properties. The effect of several dopant elements such as Al, In, Cu, Fe, and Sn on the microstructure of ZnO thin films has been investigated in detail in reference 55.

In Reference 21 several of the specimens giving rise to SHG response were doped with indium. However, a particular effect due to the doping is not addressed, and it is reported that the doped samples do not break the general trend of the undoped samples.

More importantly, a comprehensive description concerning variations in structural, morphological, optical, as well as nonlinear optical (NLO) properties induced by F as dopant element, has been reported in Reference 38. Here, the F atoms are incorporated effectively in ZnO films deposited by a chemical deposition technique. The SHG response of fluorine-doped ZnO thin films (ZnO:F), having thickness in the range 530-570 nm, is investigated with particular attention to the effect of substrate temperature on the morphological, optical, and nonlinear optical (NLO) properties. Maker fringes technique in transmission mode was employed for second (SHG) and third harmonic generation (THG) measurements. From the point of view of crystalline structure, XRD evidenced a preferential growth along the ZnO (0002) plane and a corresponding average crystal size of less than 32 nm. It was found that the substrate temperature affects the morphology of the surfaces as well as

some optical properties. The films deposited at the lower temperature (400 °C) showed a uniform surface covered with needle-like grains as well as efficient SHG and THG response. The highest values of the evaluated nonlinear $\chi_{eff}^{(2)}$ coefficients were found for the sample deposited at lowest temperatures, as reported in Table IV: $\chi_{31}^{(2)}$=10.3 pm/V and $\chi_{33}^{(2)}$=26.4 pm/V (400 °C) [38] and $\chi_{31}^{(2)}$=5.3 pm/V and $\chi_{33}^{(2)}$=16.4 pm/V (425 °C) [56]. The increase of substrate temperature negatively affects the observed SHG intensity. On the contrary, for films deposited at 525°C, a porous surface with irregular-shaped grains was obtained and a lower value of the SHG and THG response was observed. As already mentioned, this circumstance should be directly connected to the crystallite sizes which is correlated to deposition temperature. As the substrate temperature increases, a slight increase in the crystallite size of the films occurs, from 26 to 35 nm, thus reducing the density of grain boundaries and interfaces that contributes to the SH response. Furthermore, authors observed that the incorporation efficiency of F decreases markedly with increasing substrate temperatures due to vaporization, thus reducing the efficiency of incorporation of F atoms within the film texture.

In Reference 57 highly epitaxial Al-doped ZnO, grown by RF magnetron sputtering on sapphire is investigated. Typically, Al dopants are introduced to achieve n-type ZnO (Al:ZnO) [58]. Femtosecond Ti:Sapphire laser at the near-resonant SH wavelength was employed for RSHG measurements at two different incidence angles (45.0° and 20.4°). Further SH curves were taken as a function of fundamental beam polarization angle.

The ratios between the nonlinear coefficients were retrieved from the experimental results. The high value obtained for the ratio d_{33}/d_{31}=25.6, shows that d_{33} is the dominant component of the nonlinear susceptibility tensor. At the same time, the ratio d_{15}/d_{31}=2.72 confirms the deviation from Kleinman's symmetry ($d_{15}=d_{31}$) in the Al:ZnO films, due to the absorption at SH wavelength (405 nm). Absolute values of non linear optical components were found to be d_{15}=0.35 pm/V, d_{31}=0.13 pm/V and d_{33}=3.27 pm/V [57] (see Table IV).

The effect of three different ions, He, Cu and Zn, implanted into ZnO single crystals at different temperatures was investigated in Reference 59. Due to their different weight and radius, the

ions reach different penetration depths, the deepest implantation is achieved for He. Authors employed Ti Sapphire tuned at 840 nm, at an incidence angle of 26°, and observed both band edge emission (396 nm) and SHG (420 nm). By comparing the ratio of the integrated intensity SHG signal to that of the band edge, it is found that for He^+ implantation this ratio increases by 16% (17% after annealing). Using Zn implantation produces an increase of 23% (which drops to 12% after annealing), while Cu implantation does not have significant influence on SHG efficiency. As a confirm, the XRD curves of the samples show that Cu-implanted ZnO has a rocking curve analogous to the as-grown ZnO. In contrast, the rocking curves of He- and Zn-implanted samples show several satellite peaks beside the (0002) peak of hexagonal ZnO, indicating the formation of coarse grains and quasi-interfaces in these ion implanted samples [59].

SHG, along with open and closed z-scan measurements, were performed on Mn doped and Mn–Al codoped ZnO thin films grown onto glass substrate by the spray pyrolysis technique [60]. SHG from a fundamental beam tuned at 1064 nm show the dependence of the nonlinear optical parameters on the Mn concentration, while the maximum efficiency is reached for Mn doping of 5%. The photoinduced SHG is caused by different factors such as ZnO nanocrystallites, Mn transition metal, thermoheating effects and phonon subsystem.

Finally, the mentioned examples show that doping with several elements such as F [38], Al [57], He [59], Zn [59] and Mn [60], opens the way to SHG enhancement. The formation of quasi interfaces inside ion implanted samples introduce a contribution of these symmetry breaking interfaces resulting in an improvement of the SHG efficiency.

IV. SHG FROM ZNO NANOWIRES/NANORODS

With the increasing progress in technology and characterization techniques, several ZnO nanostructures have been developed and synthesized as nano-objects, having potential applications in making optoelectronic devices.

Among the enormous variety of ZnO nanostructures, undoubtedly nanorods and nanowires have been the focus of most studies since their geometries allow the preparation of arrays of well controlled uniformity, shape, and size distribution. As well as for ZnO films, second harmonic generation from ZnO nanorods and nanowires grown by different methods has been widely investigated. Nucleation with gold-seeded sapphire substrate [61], aqueous solution method [62-65], modified aqueous chemical growth method [66], vapor-liquid-solid technique [67] or chemical phase vapor deposition [68] represent only few examples. At the same time, many efforts have been made to quantitatively determine the second-order nonlinearity of both single ZnO nanorod/nanowireand arrays. In particular, Table V synthesizes all the experimental results that are reported in this section and sub-sections. The main outcome of these studies is represented by a considerable enhancement of second-order nonlinearity of ZnO nanostructures in comparison to bulk and thin film materials. This feature is generally ascribed to the fact that one dimensional (1D) semiconductor nanostructures have high surface to volume ratios, resulting in enhanced effective surface dipole moments, particularly in the radial direction of ZnO rods.

Concerning with the crystalline structure, it is commonly considered wurtzite for the nanorods, nanowires and nanostructures in general, as well as for ZnO films. The same non-vanishing elements of the nonlinear optical tensors are thus investigated and characterized. Considering orientation direction, the nanorods are most frequently oriented with the main axis perpendicular to substrate surface (*c*-axis), as shown in Figure 9(a). Given this orientation, the $d_{zxx}=d_{31}$ is excited when the fundamental beam electric field oscillates along the radial direction of nanorods. This term in ZnO nanorods and nanowires becomes significantly higher with respect to films, because of the high surface to volume ratio which in turns results in large effective surface dipole moments in the radial direction of ZnO rods. Nevertheless, the maximum SHG signal for rods and wires occurs when the polarization is along the nanowire symmetry axis, in which case $d_{zzz}=d_{33}$ is excited and probed [61].

In a few cases, the nanorods are disposed with their axes parallel to substrate surface [61-63]; under these conditions it was possible to isolate the contribution of the single nanocomponent.

The microscopic second-order nonlinear coefficient of a single nanowire was measured for the first time by near-field scanning optical microscopy (NSOM) [61]. The nanowires were dispersed onto a flat sapphire substrate, thus their axes were parallel to the substrate surface. Oblique collection mode NSOM, using a fundamental beam tuned at 800 nm for SHG and 1320 nm for THG, was used to image both SHG and THG from single ZnO nanowire, and a large nonlinear response was demonstrated. A strong polarization dependence was evidenced by the SHG images which is ascribed to the asymmetry of the nonlinear susceptibility. The values of the nonlinear optical tensor were found to be $\chi^{(2)}_{31}$=2.5 pm/V and $\chi^{(2)}_{33}$=5.5 pm/V, in agreement with ZnO thin films although lower than the reported bulk value of χ_{33}=-14.31 pm/V [62]. The relatively low values retrieved in this work is ascribed to the high number of molecules in the ZnSe reference sample, far exceeding the restricted number of ZnO molecules probed for a single ZnO NW [61].

In many circumstances SHG provides a useful contactless tool to monitor structural defects, as twinned structure in rods. As well as for ZnO films, if defects as twinning are present in nanorods, they can be experimentally investigated using SHG [63]. ZnO rods (length of several microns and diameter 100-250 nm) grown with the aqueous solution method were disposed with their polar axes parallel to the surface of fused quartz, as shown in Figure 9(b). A Ti:sapphire laser (100fs) tuned at 810 nm was employed as pump beam. The far-field scattering patterns of the transmitted SH waves from single twinned rod was compared to the pattern arising from a twin-free ZnO rod in order to see if it is possible to discriminate the differences between twinned and twin-free ZnO rods. Very interestingly, the distribution of the interference fringes in the scattering patterns appeared to be strictly connected to the twinning structures inside the rods. In particular, the zero-angle fringes highlight the different features of the two kinds of rods. A dark (bright) fringe at the 0° scattering angle was revealed and ascribed to destructive (constructive) interference of the SH electromagnetic waves emitted from each halve of the twinned (twin-fee) rods. Furthermore, it is found that the number of the interference fringes decreases as the length of the rod is reduced [63].

The pattern of the SHG polarization diagrams measured from forward transmitted irradiation, instead of the commonly measured backward -or reflected- irradiation, was employed to determine the second order susceptibility tensor of ZnO rods grown by the aqueous solution method [64]. Rods were several microns long with a diameter of 100-250 nm. Their axes were oriented parallel to the fused quartz substrate surface, and their density was very low, so it was possible to excite only one rod during experiments. Using a Ti:Sapphire tuned at 810 nm (100 fs), the strongest SH signal was measured for p-p polarization configuration. Authors found the ratios: d_{33}/d_{31}=-5.4 and d_{15}/d_{31} =1.53. indicating that d_{33} is the dominant component and has an opposite sign with respect to the other tensor components. Concerning the absolute values it was found d_{33}=3 pm/V,d_{31}= 0.56 pm/V and d_{15}=0.86 pm/V. It's worth to note that Kleinman symmetry does not hold in this case, most likely due to the absorption of the SH radiation at 405 nm [64].

The most important feature making one dimensional (1D) semiconductor nanostructures, as nanorods and nanowires, interesting is their high surface to volume ratios. SHG can be useful as a surface investigation tool for nanorods characterization. High quality and nearly vertically aligned ZnO nanorods arrays were grown onto a ZnO-seeded glass, by aqueous solution method (100 nm diameter and 1 μm length) [65-66]. During the growth of ZnO nanorods, oxygen deficient defects are spontaneously generated. These defects are responsible for reduced optical properties since they suppress the UV emission efficiency, thus degrading the performances of photodetector devices, for instance. Some authors performed a post-annealing process (800°C) in order to reduce defects, while the second order nonlinear optical properties were characterized before and after annealing [65]. SHG was measured in the Maker fringes scheme in transmission mode, using an Ytterbium laser tuned at 1044nm (280 fs pulses time duration). The strongest nonlinear optical tensor element d_{33} was characterized and it was found d_{33}=0.4 pm/V for the "as-grown" sample, which becomes larger after the annealing treatment, d_{33} =0.65 pm/V [65].

Similarly, same type of ZnO rods where investigated with analogous experimental setup, using several post-annealing temperatures (between 600°C and 800°C) in order to reduce defects [67]. It was

found that d_{31} increases with increasing annealing temperature, or equivalently the ratio d_{33}/d_{31} decrease from 1.11 (as grown sample) to 0.91 (annealed at 800°C). At increasing annealing temperature the oxygen vacancies concentration decreases, improving both the crystal quality and the conductivity of the nanorods [66].

Also ZnO nanostructures can be doped by adding some suitable elements during the preparation process. In case of doping with rare earth elements, a stable and sharp luminescence in a range of visible to near IR could be achieved. Europium is a very interesting rare earth element and has been used as an effective phosphor for its strong red luminescence. ZnO nanowires were grown by modified aqueous chemical growth method onto quartz substrate, using europium nitrate for the doping process [67]. For comparison, undoped ZnO nanowires were prepared using the same process, without doping precursor. Highly crystalline nanowires with diameters 70-100 nm and length of few microns were obtained along the *c*-axis (perpendicular to the substrate), while no significant changes in the diameter and length of the ZnO nanowires was revealed with an increase in the Eu content. Due to the larger ionic radius of Eu ions, with respect to the Zn ions, the incorporation of the Eu ions caused the expansion of the lattice, which is evidence by a small shift in the XRD [67].

The SHG emission from a linearly polarized Ti sapphire (800 nm, 70 fs) was detected by Maker's fringes method, using *p-p* polarization configuration. A strong SHG was observed at 400 nm from both undoped ZnO and Eu:ZnO nanowires. The magnitude of SHG from the undoped ZnO nanowires was found to be improved by Eu doping. The maximum SHG was observed for the 1% of Eu ions ZnO nanowires, being about 4.5 times larger than the undoped ZnO nanowires. In particular, a strong correlation was found between the maximum d_{eff} and the so called asymmetric factor, which gives an indication of lattice distortion [67]. The highest d_{eff} =19.09 pm/V was obtained for 1% Eu doped ZnO nanowires, which is comparable with other results obtained from ZnO thin films by different techniques. Previous efforts to enhance SHG in ZnO thin films lead to a second order optical nonlinearity of about -15 pm/V(d_{33}) by changing the crystallographic orientation [33] or 22.5 pm/V by

decorating the surface with metal nanoparticles followed by bicolor coherent treatment [17]. In comparison, Eu doping is a much simpler technique, with respect to the mentioned attempts.

Finally, inverted microscope configuration with a Ti: sapphire laser (780-810 nm) in reflection mode was employed to investigate ZnO nanorods array deposited onto Si substrate by CVD method, whit the *c*-axis perpendicular to the surface (diameters between 100 and 500 nm) [75]. The value of near-resonant d_{15} was measured to be 10.2 pm/V at 800 nm, far exceeding that measured, also in resonant condition, by Neumann et al (2.6 pm/V) [21]. This high value is mainly ascribed to the enhancement of the exciting electric field intensity inside the nanorod. The average pump light intensity inside the volume of nanorods, in fact, was calculated to be twice the incident intensity, corresponding to a four-fold enhancement of the SHG intensity by local field effect [75].

The latter example shows how significant is the choice of pump beam wavelength. Indeed, near the absorption wavelengths, Kleinman's symmetry is broken and d_{15} results to be enhanced. However, a detailed analysis of wavelength dependence, will be the object of the following section.

A. WAVELENGTH DEPENDENCE

SHG from ZnO nanostructures often appears together with THG as well as with multiphoton excited photoluminescence (MPL). Considering the different nonlinear optical processes, their competition and possible energy exchange strongly depend on both fundamental beam wavelength and intensity. As a consequence, SHG may be depleted by various channels, thus a detailed study is necessary in order to separate (distinguish) the different contribute to the emitted radiation.

MPL generically includes photoluminescence following two photon absorption (2PA), three photon absorption (3PA) and so forth. In several works the competition between SHG and two-photon absorption (2PA) and/or 3PA has been deeply discussed. Changing the fundamental beam wavelength is a useful way to highlight the different contributes to the emission spectrum. While SH wavelength changes accordingly to change in fundamental beam wavelength, for MPL wavelength it is fixed by

the ZnO band gap. On the other hand, concerning with the competition between SHG and THG, the intensity of SHG scales quadratically with the pump intensity while the intensity of the THG exhibits a cubic dependence on the excitation intensity. As a consequence, varying the excitation intensity is suitable approach to monitor the competition between SHG and THG.

Furthermore, since ZnO has a large exciton binding energy of 60 meV, an efficient exciton emission can be easily observed under low excitation energy. A resonant enhancement of the SHG can be induced when the pump beam energy is higher than half the band gap.

In [68] SHG and exciton, by two photon absorption (2PA), are simultaneously generated in a single isolated ZnO nanowire. The fundamental beam is a tunable Ti:Sapphire laser (100 fs) in the wavelength range 600-900 nm. Interestingly, authors chose different energy (wavelengths) for the resulting generated beam: above the band gap (for pump beam tuned at 700 nm), near the band gap (720 nm), near exciton (753 nm) and below the band gap (800 nm). Experimental results show that SHG is significantly enhanced when the generated wavelength is tuned near the exciton wavelength, i.e. if pump beam is set to 753 nm. This enhancement is attributed to the energy transfer between the exciton and the SHG. Actually, detuning the pump wavelength from this resonance peak to either upper or lower wavelength results in a decrease of the SHG intensity. In addition, at 753 nm the slope of the SHG signal as a function of pump intensity is found to be 3.2, much higher than the typical square dependence, which in turn is obtained when pump is tuned at 700 nm [63].

The photoluminescence (PL) emission properties of ZnO nanowires (having diameter 100-300 nm and length 10-30 μm) excited by intense femtosecond pulses was investigated in [69]. ZnO nanowires were prepared by chemical phase vapor deposition using an Ag film as catalysts onto silicon substrate. Samples were excited in the range 780-830 nm (150 fs) and their emission was detected by a spectrometer at room temperature. The interesting emission plot which is reprinted in Figure 10 shows the emitted radiation of ZnO nanowires excited using a fundamental beam tuned at 806 nm and measured with a tilt angle of 30°, as a function of wavelength. In particular, three peaks are clearly distinguished, corresponding to SHG at 403 nm, to oxygen vacancies defects at 500 nm and

at 385 nm (=3.22 eV). The latter could be attributed to the recombination of exctions through the exciton-exciton collision process that is often called P-band emission. Here, despite the laser pulses have photon energy less than the half of the band gap, the intense light-matter interaction (peak power 10^{11} W/cm^2) still makes possible to generate PL emission via 2PA process [69].

Because of the high refractive index of ZnO within the whole visible spectral region (n>2), ZnO nanowires are suitable sub-wavelength waveguides providing tight optical confinement for low-order modes. Their potentiality as waveguiding nano objects has been explored in both arrays of ZnO nanowires and single ZnO nanowire (diameter 100 nm and length of about 2 μm), grown by a wet chemical synthesis method. Fundamental beam wavelength was tuned between 700 and 900 nm (pulse duration of 50 fs). Furthermore, the efficient and broad internal photoluminescence obtained in single nanowire was employed to perform a single-nanowire transmission experiment. It was actually observed that the typical PL peak in the emission spectrum undergoes a red shift with increasing time, due to band gap reduction induced by the local heating due to fs pulses [70]. However, SHG exhibited relatively low efficiency, mainly ascribed to the unfavorable excitation direction, which in this case was perpendicular to waveguide direction [70].

Very often emission spectra from a bulk ZnO crystal are compared to those obtained from a thin layer of nanowires or nanorods and the problem of isolating the SHG response from the detected signals (first of all PL) is promptly addressed [71]. For SH wavelengths near the band gap, multi photon luminescence (MPL) has to be taken into account and two-photon luminescence dominates the emission spectrum. For SH wavelength above the band gap, i.e. when the fundamental beam wavelength is longer than 2·367 nm,the emitted light is dominated by SHG.

The competition between 2PL and SHG is clearly described in Reference 71, where randomly oriented ZnO wires grown on an Si/SiO_2 wafer and on quartz substrate are investigated and compared with a bulk ZnO sample. SHG from nanowires was measured in reflection mode using an OPO pumped by Nd:YAG laser (6 ns). The p-polarized pump beam was tuned in a wide spectral range, from 710 to 1000 nm, using narrow step of 10 nm. The results obtained from ZnO nanowires is the

remarkable, representative contour plot which is shown in Figure 11, where the intensity of the emitted signal is reported as a function of both the pump wavelength (*x*-axis) and the emission wavelength (*y*-axis) [71]. The SHG signal is clearly visible as the diagonal line tuned at half the pump wavelength. The weaker horizontal line is the multiphoton excited photoluminescence (MPL). When the PL appears at wavelength shorter than the SHG, i.e. below the line of SHG, it is most likely due to (weak) three photon luminescence. On the other hand, the much stronger two-photon process is seen above the SHG line. The oxygen vacancies defect emission, i.e. the weak peak tuned at 500 nm, is clearly identifiable only when pump beam wavelength is more energetic (<710 nm) [66].

The raw SH intensity spectra from the nanowires film and the bulk crystal are quite different, since strong PL only appear for the nanowires sample. However, despite the lack of photo luminescence signal, also the bulk ZnO reference sample produce a sharp peak of d_{eff} values when the pump beam wavelength is such that the corresponding SH is resonating in the band gap [71].

Monitoring the intensity dependence of generated signals, in a useful way to understand the competition between SHG and THG. In particular, SHG should be dominant at low excitation intensities, while THG prevails at increasing excitation intensities [72]. In order to have both nonlinear optical processes, a pump wavelength longer than 1100 nm is preferred, so to avoid 3PA of the pump beam as well as single photon absorption of the resulting THG.

In Reference 69 an excitation beam tuned at 1350 nm, was employed to investigate the competition between SHG and THG by two approaches, i.e. either moving a lens placed before the ZnO nanorods sample or by tuning the fundamental beam wavelength [69]. The ZnO nanorods have diameter of 250 nm and length of 2 μm and are compressed into a film with a thickness of 100 μm. The change from SH to TH regime is clearly noticed in the transition from a red to a blue spot onto the sample surface, as the focusing lens is getting closer to sample. It is also observed that the THG intensity decreases with decreasing excitation wavelength, mainly due to material reabsorption. In particular, a significant reduction occurs when the pump wavelength approaches 1150 nm, since the corresponding THG energy (383,33 nm=3,23 eV) becomes higher than the exciton ground state [71].

Due to energy redistribution, a progressive saturation is observed for both SHG and THG. Considering the dependence on excitation intensity, the slope derived for SHG was initially 1.80 and for THG 2.83. At intensity of about 0.25 TW/cm^2 THG becomes stronger than SHG. When intensity is further increased (up to 0.513 TW/cm^2) four photon absorption (4PA) arises and a broad peak at 390 nm appears in the spectrum, whose intensity increases with increasing pump intensity, due to exciton emission resulting from the 4PA, i.e. four photon luminescence (4PL).

In a different spectral range, i.e. for SH wavelength around the band gap, there exists a competition also between SHG and 2PL which strongly depends on the excitation intensity [73-74]. For a deep understanding of such a competition in ZnO nanorods (200 nm diameter and 2 μm length), the pump beam (130 fs) wavelength was chosen to be 754 nm=1,64 eV [73]. Since the energy of 2 pump beam photons (3.28eV) is slightly larger than the exciton ground state but still smaller that the bandgap energy of ZnO (3.37eV), it was possible to have 2PA (and afterwards 2PL) [73].

The nonlinear optical responses of single, double and multiple (clusters) ZnO nanorods under the excitation of fs laser were systematically investigated [73]. Experimental results point out that for single ZnO nanorod only SHG was observed, even at the highest excitation intensity. In sharp contrast, a rapid increase in 2PL was observed in the double and multiple ZnO nanorods and, moreover, at high excitation intensities their nonlinear response spectra became completely dominated by 2PL. This difference in the nonlinear optical response of single and multiple ZnO nanorods was explained by considering both the electric field distribution and the heat accumulation effect. The significant enhancement in electric field intensity in the multiple ZnO nanorods, which was also confirmed by numerical calculations, is thought to be responsible for the enhancement in 2PA and consequent 2PL. On the other hand, the absorption itself increases, due to the thermally induced bandgap reduction, and contributes to the significant enhancement in 2PL observed at high excitation intensities [73]. If the pump beam wavelength is increased, i.e. above 770 nm where 2PA is not energy-allowed, SHG is the dominant process [73-74].

In Reference [74] the excitation wavelength was tuned from 750 to 795 nm so that excitons could be selectively generated via 2PA above or below the exciton ground state of ZnO nanordos. At high excitation intensities, the nonlinear response spectrum became dominated by 2PL for excitation wavelengths shorter than 770 nm, whereas it was still governed by SHG for excitation wavelengths longer than 770 nm. More interestingly, a negative slope, which indicates a reduction of SHG with increasing excitation intensity, was observed at high excitation intensities for excitation wavelengths longer than 770 nm, implying the energy redistribution or energy transfer between SHG and 2PL [74]. A minimum negative slope of -1.54 is found when pump beam is tuned at 790 nm, being this the first experimental observation of negative slope for SHG vs intensity [74].

In conclusion, all the mentioned works on SHG from ZnO nanowires and nanorods show that considering SHG process is not exhaustive. The deep understanding of the nonlinear optical processes, wavelength- and intensity-allowed, and the competition between them are fundamental for controlling and engineering the nonlinear optical applications ofZnO nanowires and nanorods.

B. ASPECT RATIO

Nonlinear optical properties of ZnO nanordos are strongly influenced by their dimensions including length, diameter and aspect ratio. Size-dependent second harmonic generation (SHG) in ZnO nanorods has been investigated in several works, however a detailed description to the SHG dependency with nanorods dimensions has yet to be given.

The effect of different rods aspect ratio was explicitly investigated in Reference 76. ZnO nanorods were grown perpendicularly to glass substrate by an aqueous solution method. It must be pointed out that, if compared with polycrystalline ZnO thin films, ZnO nanorods possess higher uniformity and order with well-defined nanorod’s length and diameter. Therefore it was possible to select different aspect ratios, defined as length to diameter ratio, ranging from 5.7 to 10.8. The effect of increasing rod’s length is evident also in transmission spectra in the visible range, since a transmission

decrease near the band-edge is observed with increasing rods' length, due to scattering in the transmission region [75]. SHG was measured from a ns Nd:YAG laser and it was found that both d_{31} (from 0.14 pm/V to 2.88 pm/V) and d_{33} (from -7.8 pm/V to -18.0 pm/V) values increase with increasing aspect ratio.

This SH enhancement is closely related to local field effects associated to the elongated nanorod structure. As already mentioned, when pump beam is polarized along rods diameter only the d_{31} component is excited. On the other hand, being d_{33} excited along the rods longitudinal axis, the local field effects enhancement is predominantly connected to the rod's length [76].

This effect of enhancement of the nonlinearity related to the rods' length, mainly ascribed to local field effects, was also investigated in Reference 77 where similar results are discussed. Three different nanorods samples were grown on glass substrate by low temperature chemical bath method, having diameter 56, 59 and 95 nm, and length 1300, 870 and 1020 nm, respectively. Laser pump beam wavelength was 806 nm (pulse duration of 13 fs). From SHG measurements the d_{eff} was retrieved and it was found a correlation with rods' length: for the longest rods d_{eff}=15 pm/V, for the shortest rods: d_{eff}=2pm/V, and for the last sample: d_{eff}= 3.2 pm/V [77].

Furthermore, in each sample the nanorods are not exactly perpendicular to the substrate surface, but possess a different tilt-angle. A deep investigation of the angular dependence of the SHG signal (Maker fringe) revealed that the efficiency depends on the rods' tilt angle. If the polarization direction of the fundamental beam was parallel to the axis orientation, the efficiency was smaller [77]. On the other hand, the maximum efficiency was obtained when the polarization for both fundamental and generated beams is perpendicular tothe rod tilt axis, i.e., in p-p-polarization. Considering the incidence angle where the maximum SHG signal occurs, it also depends on the nanorods' structural parameters, in particular, the smaller the aspect ratiobetween rods' length and diameter, the smaller the angle for SHG maximum [77]. A similar behavior was reported elsewhere for nanosecond pulse excitation [76].

In [78] ZnO nanorods were grown by hydrothermal method on indium tin oxide (ITO) glass plate. Four diameter/length combinations were selected: 60/360, 90/1700, 100/950, 280/3700, with their longitudinal *c*-axis perpendicular to substrate surface. The relationship between rod diameter/length and the corresponding $\chi^{(2)}$ values based on Lorentz local field is established both theoretically and experimentally for the first time.

The so-called Lorentz local field effect arises from the difference between the refractive index of the particle, ZnO nanorod in the present case, and the surrounding dielectric, thus resulting in enhanced field intensity at the particle surface (boundaries) [78]. In solid state materials this effect was verified on ZnO nanorods [75]. From the theoretical point of view, the Lorentz local field induces a spectral red-shift as well as a consequent dielectric constant modification, which are used to explain the size effect for $\chi^{(2)}$ in the off resonance regime.

A far from resonance laser wavelength was employed for SHG measurements (1034 nm, 430 fs), thus Kleinman symmetry is assumed to be valid. The obtained values for $\chi^{(2)}_{31}$ are discussed as a function of rods' diameter while the values of $\chi^{(2)}_{33}$ are correlated to rods' length. The outcome is an experimental evidence that $\chi^{(2)}_{31}$ grows with increasing rod diameter (from 0.59 pm/V to 1.98 pm/V). The theoretically calculated curve saturates to the value of 4 pm/V when diameter approaches the value of 1 μm, i.e. it reaches the value of bulk ZnO. This result implies that bulk contribution exceeds surface local –Lorentz- field contribution. On the other hand, $\chi^{(2)}_{33}$ was investigated as a function of rods' length and its value is found to grow with increasing rods' length (from -2.77 pm/V to -19.06 pm/V). Further increase of rods' length would lead to an upper bound also for $\chi^{(2)}_{33}$, exceeding that of bulk ZnO (-14 pm/V) when the length is higher than 1 μm. This result is an indication that Lorentz local field is stronger along the longitudinal axis.

Both mentioned works show that increasing the aspect ratio has more influence on d_{33} than on d_{31}. Nevertheless, a reliable evidence connecting SHG efficiency with nanowires aspect ratio is still requiring more and statistically relevant data.

C. SHG IN ZNO NANOSTRUCTURES

Beside the large amount of works on ZnO nanorods and nanowires, several other nanostructures have been developed and their nonlinear optical properties characterized.

Tree-like microcrystalline structures, as shown in Figure 9(c), were obtained starting from a ZnO hexagonal wire, through a hydrothermal method [80]. The obtained nanostructure consists of hexagonally organized six columns of branched nano/microwires, with the lateral sizes of the wires inthe range of 50–400 nm and length of about 2-3 μm. As a wide band gap semiconductor, ZnO has three excitons band gaps at room temperature, namely A (3.309 eV), B (3.315 eV) and C (3.355 eV). Among them, A and B excitons mainly respond to radial solicitation, i.e. to electric field polarized perpendicularly to the wires'axis, while the C exciton is only allowed for axial direction of the electric field. In other words, if light beam is normally incident onto a nanowire axis, and it is polarized along the wire (E ∥ *c*-axis), the electric dipole transitions are such that the C exciton is strongly active whereas the B exciton is very weak and A exciton is forbidden. If the polarization of the incident light is perpendicular to the wires'axis both A and B excitons are active while the C exciton is forbidden.

Due to the hexagonal symmetry of the original nanostructure, the polarization of the incoming light with respect to the wires *c*-axes can be at the same time parallel –for some wires- and perpendicular –for others-, so that all three exctions (A B and C) of ZnO can be simultaneously activated by incoming photons [80].

In Reference 81 ZnO nanocrystals with very small radius (1.8 nm) and hexagonal wurtzite structure were synthesized and embedded in polymethylmethacrylate (PMMA) starting from a colloidal solution and then by spin coating [81]. The resulting film thickness is 100 nm. The optical absorption spectrum of the material at room temperature shows the maximum of the absorption at 4.54 eV. Since the bulk ZnO band gap energy is 3.37 eV, the blue shift of 1.17 eV is ascribed to quantum confinement due to size effect [81]. Luminescence spectrum leads to three bands located at 481.5 nm, 531.09 nm and 671.28 nm. The first and second are generally attributed to oxygen vacancies defects and zinc interstitial in ZnO. The last one (671nm=1.85 eV) is attributed to surface defects.

Very high values of the nonlinear optical tensor components were retrieved, d_{33}=2.975·10^{-10} m/V=297.5 pm/V and d_{31}= -148.5pm/V, from Maker fringes curves, obtained in transmission mode using a pump beam tuned at 1064 nm (16 ps) [81]. The extremely high values are attributed to quantum confinement mainly due to the low dimensionality of crystallites of ZnO dispersed in PMMA matrix as well as to surface effects. The reduced crystallites' size allows quantization of energy levels, enlargement of band gap and the creation of excitons. When excited with field associated to the incident wave, these electron-hole pairs create dipoles [81], contributing to the nonlinear optical signal.

Recently, ZnO nanoparticles have been successfully investigated for possible applications in biological imaging. It was shown that ZnO nanoparticles can be used as biological marker for cell tracking (Zebrafish cells) and imaging for extended observation times [82]. From the linear optical point of view the use of ZnO as a biological marker is difficult, but its nonlinear properties makes its use more attractive. Unlike multiphoton emission, in fact, SHG do not present nonradiative decay pathways that may cause thermal heating of the cell, thus allowing for long time tracking and imaging without cell damage. Furthermore, the SHG created in nanoparticles can be very efficient and can be tuned to the biological windows of the cell, in order to avoid autofluorescence by the proper choice of the excitation wavelength.

Arc vapor technique was employed to create a wide distribution of particle sizes and shapes of ZnO nanoparticles (10 to about 300 nm), and then a dense colloidal solution was prepared. The SHG of highly optical nonlinear ZnO nanoparticles was used for in vitro biological imaging. As a disadvantage, the SH generated signal can also be dominated by the 2PL photoluminescence process if the energy of the pump wavelength exceeds half of the band gap of the ZnO semiconductor. Since 2PL can be detrimental to the imaging process due to thermal dissipation, it should be avoided for biological samples by choosing the convenient excitation wavelength, ie. $\lambda_{pump} > 2\ \lambda_{BG}$ [82].

Authors of [83] suggested Hyper Rayleigh Scattering (HRS) technique to retrieve ZnO nanoparticles nonlinear optical properties, using a Nd:YAG laser (1ns). Polarization resolved HRS was used to retrieve nonlinear optical tensor components that have been fed as input parameters to interpret

the following SH microscopy measurements of same particles: two different ZnO nanopowders, having particles' diameters of 20 nm and 200 nm, were dispersed into water or ethanol. It was found that the average nonlinearity obtained for both ZnO 20 nm (d_{xxx}= 0.7-1.8 pm/V) and ZnO 200 nm (d_{xxx}=1.1-2 pm/V) are rather low and very similar despite their difference in size [83].

An original form of nanostructure is the nano-sized tetrapod, whose SEM image is shown in Figure 9(d) [84]. The tetrapods were synthesized by evaporating Zn powder in a quartz tube at 950 °C. Typically a tetrapod structure is composed by four arms with lengths of several microns and widths up to 80 nm. High quality single crystalline nature of the tetrapods was demonstrated via XRD. SHG was observed from single nano-sized ZnO tetrapod and then compared to a bulk ZnO single crystal [84] in the wide wavelength range 710-930 nm using fs source.

Surprisingly, it was found that the SHG arising from nanotetrapods is over two orders of magnitude stronger than that of bulk single crystals. Moreover when the energy of the excitation photons is lower than half the band gap of ZnO, i.e. at long wavelengths, SHG becomes predominant with suppression of band edge luminescence in the tetrapod. On the other hand, a residual 2PL keeps remaining in the bulk ZnO reference sample [84].

Comparison between tetrapods and bulk crystal was performed at several wavelengths, 730, 790, 830 and 850 nm. Excitation at 790 nm is particularly important since the SHG signal just coincide with the band edge emission centered at 395 nm at room temperature. If wavelength is shorter than 790 nm, a band edge emission at 395 nm and a broad green emission centered at 500 nm were observed from both tetrapod and bulk crystal, being the band edge PL and green emission from the bulk stronger than from the tetrapod. When the wavelength is tuned to 790 nm the coherent SHG emission is in resonance with the band edge emission at 395 nm. Despite resonant enhanced SHG was already observed [67], such a resonant enhancement effect for the tetrapods was observed with a strong suppression of both the band edge emission and the green band, while the enhancement is not noticeable from the bulk ZnO. The unique tetrapod structure with large boundary surfaces is responsible for SHG enhancement. Their four long arms provide a huge effective structural symmetry

breaking surface area. Furthermore, unlike the common resonant effects, the SHG signal did not drop when the excitation wavelength was further tuned. Indeed, in addition to the signal generated by the ZnO structure (6mm), a large contribution of SHG can be generated at grain boundaries and film surfaces, as already pointed out by Cao et al [19].

On a different scale, efficient SHG was experimentally observed from bigger structures, namely hollow ZnO rods having diameters of 200 μm and length of a few millimiters [85]. A fs laser tuned at 774 nm was employed to excite SHG. The incident plane was perpendicular to rods' *c*-axis, and incidence angle is 26°. The SH arising from the hollow ZnO sample was found to be much stronger with respect to the reference sample (a thick ZnO solid rod). Furthermore, the dependence of the SH was investigated as a function of several parameters, as pump beam power, polarization angle and emission wavelength. The enhancement of SHG signal is attributed to the multiple total reflections between the outer and inner surfaces of the sample, giving a ninefold amplification factor, which can be a positive issue for nonlinear optical devices fabrication.

V. THIRD HARMONIC GENERATION-THIRD ORDER NONLINEAR OPTICAL EFFECTS

We finally wish to conclude the present review giving some information on third order nonlinear optical processes from ZnO films and nanostructures.

In analogy with SHG, third harmonic generation (THG) is responsible for the frequency tripling of the incoming beam at ω, via the third order susceptibility, $\chi_{ijkl}^{(3)}(-3\omega, \omega, \omega, \omega)$ which is a fourth rank tensor. In most of the cases, third harmonic generation is investigated via the Maker fringes technique. As well as for SHG, the Maker fringes curves of the generated signal at 3ω, allow to retrieve the components of the fourth rank tensor $\chi_{ijkl}^{(3)}$. The non-zero components of the third order susceptibility can be addressed by choosing different polarization states for fundamental and generated beam, respectively.

Being third order nonlinear optical phenomena related to an odd powered term in the nonlinear optical polarization, THG is symmetry allowed in all materials, including air. As a consequence, during THG measurements, the sample has to be kept under vacuum to avoid spurious contributions.

The number of works on third harmonic generation (THG) from ZnO films and nanostructures is limited, with respect to those on SHG. The main reason is that the third order nonlinear susceptibility is about 10 order of magnitude lower than the second order one, and –moreover- the TH wavelengths typically appear in the UV region, where detection is not easy and reabsorption plays an important role [72]. We show the variability of THG data in Table VI.

The fourth rank nonlinear optical tensor $\chi_{ijkl}^{(3)}$ for the 6*mm* point group symmetry presents two components, namely$\chi_{1111}^{(3)}$ and $\chi_{3333}^{(3)}$. For ZnO films deposited along the (0002) planes, i.e., with the axis mainly normal to sample surface, it is possible to investigate the $\chi_{3333}^{(3)}$ by selecting the p_{ω} - $p_{3\omega}$ polarization configuration. In Reference 28 the third order susceptibility, $\chi_{3333}^{(3)}$, was evaluated for ZnO samples grown by dual ion beam sputtering. Maker fringes technique was applied, at a fundamental wavelength of 1907 nm and a value for $\chi_{3333}^{(3)}$ of 1.32×10^{-12}esu, corresponding to 1.85×10^{-20}(m^2/V^2), has been found.

A strong third order nonlinear optical coefficient, $\chi^{(3)}$ of 1.4×10^{-12} esu, was measured from ZnO films grown by pulsed laser ablation, allowing the generation the third harmonic of ultrashort pulses with the efficiency of percent [36].

In Reference 38, the highest cubic nonlinear optical coefficients was evaluated via Maker fringes experiments from fluorine doped ZnO films, and it was found $\chi^{(3)}_{ZnO:F}= 0.72\cdot10^{-12}$ esu, i.e. $\chi^{(3)}_{ZnO:F}= 1.0\cdot10^{-20}$ (m^2/V^2). The same magnitude order was measured from ZnO films deposited by rf sputtering on crystal substrate, $\chi_{eff}^{(3)}$ of 0.98 and 1.22 $\times10^{-20}$(m^2/V^2), for α-BBO and $LiNbO_3$ substrates, respectively [31].

The dependence of THG on the deposition temperature was discussed in Reference 37, from ZnO films deposited by MOCVD. The growth temperature was varied between 200°C and 500°C, and

SEM investigation revealed that it strongly affects the crystalline quality of the films. For temperature <250°C smooth surface without grain formation are formed. When temperature exceeds 300°C films start exhibiting a rough surface with hexagonal grains. A further temperature increase results in columnar growth and rod formation (>350°C). In particular, the highest nonlinearity was found for a film deposited at 250°C, $\chi^{(3)}=3.77\cdot10^{-12}$ esu which is larger than that of bulk crystal $\chi^{(3)}=1.2\cdot10^{-13}$ esu. This result was explained with the increase of dandling bounds and defects in the film which in turns increase the optical nonlinearity [37].

In Reference 39 THG was observed from nanocrystalline laser deposited ZnO thin films grown at different oxygen pressure (100 and 900 mTorr, respectively) and $\chi^{(3)}$ was found to be correlated to the crystallites' size, as occurring for SHG. The smallest particle size (8 nm) produced the highest $\chi^{(3)}=9.56\cdot10^{-12}$ esu, while the biggest particle size (84 nm) provided a lower value for $\chi^{(3)}=1.2\cdot10^{-13}$ esu [39].

THG was also observed from amorphous ZnO films fabricated by dip-coating (sol-gel) method and consecutive annealing process [40]. From XRD and AFM analysis, it was observed that an annealing temperature of about 475 K leads to a crystalline change of the amorphous films. Maker fringes method in transmission mode was applied to measure both SHG and THG using a fundamental beam tuned at 1064 nm (ps). Considering THG, authors found that the $\chi^{(3)}$ of the as-grown sample $\chi_P^{(3)}=1.68\cdot10^{-18}$ m^2/V^2 and $\chi_S^{(3)}=1.60\cdot10^{-18}$ m^2/V^2 is much weaker with respect to the annealed one $\chi_P^{(3)}=7.20\cdot10^{-18}$ m^2/V^2 and $\chi_S^{(3)}=6.68\cdot10^{-18}$ m^2/V^2.

Considering ZnO nanorods, an extraordinary efficient and broadband third harmonic generation was observed in [86] from high-quality ZnO nanorods grown by low-temperature hydrothermal deposition. A strong THG signal was detected, along with suppressed SHG, while the fundamental beam wavelength was varied in the range of 1060–2120 nm. Authors investigate a couple of samples differing by the degree of nanorods alignment. In the first one nanorods are vertically aligned, yielding to a well-packed and ordered rod structure. The second sample, instead, displays less aligned nanorods

with disordered bundling. Experimental results demonstrate that THG arises from the bound electronic response of ZnO, with minimal dependence on the vertical alignment of nanorods. At the same time, the reduced SHG signals from both samples (some order of magnitude less) is ascribed to the micron-sized film thickness [23]. Furthermore, a local enhancement of the THG signal was observed for generated wavelength at 374 nm. This wavelength corresponds to 3313 meV which is very close to the free exciton energy at room temperature.

Z-scan measurements, both open and closed aperture, from vertically aligned ZnO NRs was used to determine their nonlinear refraction and absorption. In this circumstance it was found that increasing rod diameters and alignment degrees of ZnO nanorods lead to an enhancement of third order nonlinearties [87].

The rotational Maker fringes technique, using a Nd:YAG laser (1064 nm 16 ps) was employed to detect THG in s-s polarization from microrod ZnO films deposited by thermal oxidation of metallic zinc [88]. Some structural parameters, as the difference in average length of the microrods can be explained by various temperatures of annealing which have effect on the growth of the microrods [88], although in this work the annealing temperature does not affect THG. Interestingly, a higher than bulk third order nonlinearity, was retrieved: $\chi^{(3)}_{eff}$= 71 and $60 \cdot 10^{-22}$ m^2/V^2, along with negligible SHG. The lack of a strong SHG signal is ascribed to the significant scattering of the generated light on the rough surface and the relatively high film thickness (3-4 μm) [88].

Intensity dependent THG measurement along with interferometric frequency resolved optical gating (iFROG) measurements were performed on ZnO nanorods grown by high temperature vapor phase transport (VPT) and low temperature chemical bath deposition (CBD) on sapphire substrate [89]. These two deposition techniques allow to obtain similar nanorods morphologies and dimensions, even though the dissimilar deposition temperature. Ti:sapphire laser (~7 fs) with a central wavelength of ~810 nm and a wide bandwidth (>300 nm) was the exciting source. It was found that the THG efficiency of both types of ZnO nanorod samples is comparable, and significantly greater than the surface THG signal from the surface of a bare quartz sample. On the other hand, measurements of the

linear optical properties of ZnO nanorods revealed that PL emission from CBD grown ZnO nanorods results was much weaker than that from VPT grown ZnO nanorods. Finally, iFROG experimental results demonstrate the ability of the investigated ZnO nanorods films to successfully measure pulse durations below 10 fs. These studies demonstrate that ZnO nanorods films can be efficiently used to characterize pulses generated by sub-10 fs laser pulses [89].

CONCLUSIONS

In this review, recent advances on SHG from both ZnO films and state-of-the-art ZnO nanostructures (nanowires, nanorods or nanocrystals) are reported. The effect of different morphological parameters on the nonlinear properties are separately discussed in sub-sections and the values of measured nonlinear optical coefficients are summarized in Tables.

The first section is devoted to SHG from ZnO films. Film thickness is an important parameter that may significantly affect the second-order susceptibilities. Several systematic studies were performed in order to find a correlation between thickness and second harmonic efficiency in ZnO films [23, 25]. However a clear-cut dependence is yet to be demonstrated, mainly because thickness is not the exclusive factor affecting SH efficiency.

Indeed, thin films are commonly grown in a polycrystalline state which is characterized by a distribution of grains, i.e. spatial domains having the same crystal orientation. The orientation distribution within the grains results in a mean direction of the optical axis, affecting the nonlinear optical tensor components. Grain boundaries, as well as defects, represent a break in the crystalline structure, i.e. a break in the symmetry that itself can be a source of SHG. Likewise, the size of the grains plays an important role because part of the SH signal is produced at grain boundaries or by defects such as stacking faults. The effect of grain boundaries in SHG from ZnO films emerged from the experimental evidence [19] that films with lower crystallinity may show larger second order nonlinear optical response, with respect to films with higher crystallinity. So far, this and other

examples [12, 21, 26, 34, 39] have shown that, beyond the bulk, electric-dipole contribution, a significant part of the SHG signal from thin films can be generated at grain boundaries and interfaces. Following experimental results, most authors agree that decreasing both grains size and crystallinity degree, leads to enhanced SH signal.

Further research is being carried out to investigate surface contribution to SHG from ZnO films [13, 31-32, 35]. However, it must be pointed out that surface effects does not give remarkable enhancement of the second order susceptibility value, but rather change its form, introducing new non-zero elements in the nonlinear optical tensor.

Finally, significant changes in the nonlinear optical properties can be achieved by the intentional introduction of impurities within the growth process, i.e. by doping. Concerning ZnO, doping with donor impurities (n-type) is less difficult than doping with acceptor impurities (p-type), since ZnO is a naturally n-type semiconductor because of intrinsic defects such as oxygen vacancies [49]. The effect of several dopant elements such as F [38], Al [57], He [59], Zn [59] and Mn [60] on second harmonic generation efficiency of ZnO thin films has been investigated in details. Interestingly, all the mentioned experimental investigations show that doping opens the way to SHG enhancement. The formation of quasi interfaces inside ion implanted samples introduce a contribution of these symmetry breaking interfaces resulting to an improvement of the SHG efficiency.

In the second section of this review, the most prominent challenges in harmonic generation from ZnO nanostructures, are highlighted, including ZnO nanowires, nanorods and nanocrystals. Authors commonly assume the wurtzite structure for the nanorods, nanowires and nanostructures in general, as well as for ZnO films. Thus, the same non-vanishing elements of the nonlinear optical tensors are investigated and characterized.

Among the enormous variety ofZnO nanostructures, nanorods and nanowires have been the focus of most studies since their geometries allow the preparation of arrays of well controlled uniformity, shape, and size distribution. Considering orientation direction, the nanorods are most

frequently oriented with the main axis perpendicular to substrate surface (c-axis), while only few works deal with nanorods disposed with their axes parallel to substrate surface [61-63].

Several works on ZnO nanowires and nanorods show that considering SHG process is not exhaustive for the characterization of their nonlinear properties. SHG from ZnO nanostructures, in fact, often appears together with THG as well as with multiphoton excited photoluminescence (MPL). The deep understanding of the different nonlinear optical processes involved, as well as the competition mechanisms between them, are fundamental for controlling and engineering the nonlinear optical applications of ZnO nanowires and nanorods. For example, varying the fundamental beam wavelength is a useful way to highlight the different contributes of SH and MPL, the latter having a fixed wavelength dependence governed by the ZnO band gap [68-71, 73-74]. On the other hand, considering the competition between SHG and THG, the intensity of SHG scales quadratically with the pump intensity while the intensity of the THG exhibits a cubic dependence on the excitation intensity [69, 72]. As a consequence, varying the excitation intensity is a suitable approach to monitor the competition between SHG and THG.

Nonlinear optical properties of ZnO nanordos are also strongly influenced by their characteristic sizes, including length, diameter and aspect ratio. Size-dependent second harmonic generation (SHG) in ZnO nanorods has been investigated in several works [76-78]. From experimental results, it comes out that increasing the aspect ratio has more influence on the d_{33} element rather than on d_{31}. Nevertheless, a reliable evidence connecting SHG efficiency with nanowires aspect ratio is still requiring more and statistically relevant data.

Beside the large amount of works on ZnO nanorods and nanowires, several other nanostructures have been developed as tree-like microcrystallines [80], nanocrystals [81], nanoparticles [82] and nano-size tetrapod [84]. It was found either the low dimensionality of ZnO nanocrystallites [81-82] or the large boundary surfaces connected to the particular shape [84] allow to attain extremely high values of nonlinear optical coefficients.

In a separate section, we conclude this review giving some information on third order nonlinear optical processes from ZnO films and nanostructures. The number of works on THG from ZnO films and nanostructures is limited, if compared with those on SHG, due to the facts that third order nonlinear susceptibility is about 10 order of magnitude lower than the second order one, and – moreover- the TH wavelengths typically appear in the UV region, where reabsorption plays an important role [67].

In conclusions, nonlinear optical response from ZnO films and nanostructures is particularly attractive, because of the wide transparency band in the visible range and the significant and tailorable second order nonlinear response. Also, thin films and nanocomponents can be easily integrated in nonlinear optical devices. More than one order of magnitude enhancements in the nonlinear optical coefficients have been reported depending on the different possible contributions to SHG signal, as well as the large variety of preparation methods. Nevertheless, more accurate studies on fabrication and optical characterization of the samples are needed in order to take full advantage of the enhancement of the nonlinear response and to finally pave the way to possible further developments of ZnO based nonlinear sources with optimized and tailored nonlinear response according to specific applications.

REFERENCES

[1] P.A. Franken, A.E. Hill, C.W. Peters, and G.Weinreich, "Generation of optical harmonics", *Phys. Rev. Lett.***7**, 118-119 (1961).

[2] D. Passeri, M.C. Larciprete, A. Belardini, S. Paoloni, A. Passaseo, C. Sibilia and, F. Michelotti, "Second harmonic generation in AlGaN, GaN and $Al_xGa_{1-x}N$/GaN multiple quantum well structures ", Applied Physics B, 79(5), 611-615 (2004).

[3] M. C. Larciprete, A. Belardini, C. Sibilia, M.-b. Saab, G. Váró and C. Gergely, "Optical chirality of bacteriorhodopsin films via second harmonic Maker's fringes measurements", Applied Physics Letters, 96 (22), 221108 (2010).

[4] "Optics of Nonlinear Crystals", a chapter in *Handbook of nonlinear optical crystals,* ed. Valentin G. Dmitriev, Gagik G. Gurzadyan, and David N. Nikogosyan, Springer, Berlin, pp.3-65, 1997.

[5] D.A. Kleinman, "Nonlinear dielectric polarization in optical media", *Phys. Rev.* **126**, 1977-1979 (1962).

[6] M.C. Larciprete, A. Bosco, A. Belardini, R. Li Voti, G. Leahu, C. Sibilia, E. Fazio, R. Ostuni, M. Bertolotti, A. Passaseo, B. Potì and Z. Del Prete, "Blue second harmonic generation from aluminum nitride films deposited onto silicon by sputtering technique", Journal of Applied Physics 100 (2), 023507 (2006).

[7] M.C. Larciprete, M. Centini, A. Belardini, L. Sciscione, M. Bertolotti, C. Sibilia, M. Scalora, A. Passaseo and B. Potì, "Second harmonic generation in GaN/$Al_{50}Ga_{50}N$ films deposited by metal-organic chemical vapor deposition", Applied Physics Letters, 89 (13), 131105 (2006).

[8] P.D. Maker, R.W. Terhune, M. Nisenoff, and C.M. Savage, "Effects of Dispersion and Focusing on the Production of Optical Harmonics", *Phys. Rev. Lett.* **8**, 21-22 (1962).

[9] J. Jerphagnon, and S.K. Kurtz, "Maker Fringes: A Detailed Comparison of Theory and Experiment for Isotropic and Uniaxial Crystals", *J. Appl. Phys.* **41**, 1667-1681 (1970).

[10] W.N. Herman and L.M. Hayden, “Maker fringes revisited: second harmonic generation from birefringent or absorbing materials,” J. Opt. Soc. Am. B 12(3), 416-427 (1995).

[11] T.K. Lim, M.Y. Jeong, C. Song and D.C. Kim, “Absorption effect in the calculation of a second-order nonlinear coefficient from the data of a Maker fringe experiment,” Appl. Opt. **37**(13), 2723-2728 (1998).

[12] Kuang-Yao Lo, Shih-Chieh Lo, Sheng-Yuan Chu, Ren-Chuan Chang and Chang-Feng Yu, “Analysis of the growth of RF sputtered ZnO thin films using the optical reflective second harmonic generation”, *Journal of Crystal Growth* **290**, 532–538 (2006).

[13] Kuang Yao Lo, Yi Jen Huang, Jung Y. Huang, Zhe Chuan Feng, W.E. Fenwick, Ming Pan and Ian T. Ferguson, “Reflective second harmonic generation from ZnO thin films: A study on the Zn–O bonding”, *Appl. Phys. Lett.* **90**, 161904 (2007).

[14] N. Bloembergen, R.K. Chang, S.S. Jha and C.H.Lee, “Optical Second-Harmonic Generation in Reflection from Media with Inversion Symmetry”, *Phys. Rev.* **174**, 813-822 (1968).

[15] F.A. Bovino, M.C. Larciprete, A. Belardini and C. Sibilia , “Evaluation of the optical axis tilt of zinc oxide films via noncollinear second harmonic generation”, *Appl. Phys. Lett.* **94**, 251109 (2009).

[16] M.C. Larciprete, F.A. Bovino, A. Belardini, C. Sibilia, M. Bertolotti, “Bound and free waves in non-collinear second harmonic generation”, Optics Express 17 (19), 17000-17009 (2009).

[17] K. Ozga, T. Kawaharamura, A. Ali Umar, M. Oyama, K. Nouneh, A. Slezak, S. Fujita, M. Piasecki, A. H. Reshak and I. V. Kityk, “Second order optical effects in Au nanoparticle-deposited ZnO nanocrystallite films”, Nanotechnology 19, 185709 (2008).

[18] M.C. Larciprete, F.A. Bovino, M. Giardina, A. Belardini, M. Centini, C. Sibilia, M. Bertolotti, A. Passaseo, and V. Tasco, “Mapping the nonlinear optical susceptibility by noncollinear second-harmonic generation”, Opt. Lett. 34, 2189-2191 (2009).

[19] H. Cao, J.Y. Wu, H.C. Ong, J.Y. Dai, and R.P.H. Chang, “Second harmonic generation in laser ablated zinc oxide thin films”, *Appl. Phys. Lett.* **73**, 572-574 (1998).

[20] U. Griebner, R.A. Kaindl, T. Elsaesser and W. Seeber, “Frequency doubling and autocorrelation studies of 20-fs pulses using polycrystalline zinc oxide thin films”, *Appl. Phys. B* **67**, 757–760 (1998).

[21] U. Neumann, R. Grunwald, U. Griebner, G. Steinmeyer and W. Seeber, “Second-harmonic efficiency of ZnO nanolayers”, *Appl. Phys. Lett.* **84**, 170-172 (2004).

[22] A. Mitra, and R.K. Thareja, “Dependence of second harmonic generation on size of nanocrystallites of ZnO”, *Modern Phys. Lett. B* **15**, 515-521 (2001).

[23] G. Wang, G.T. Kiehne, G.K. Wong, J.B. Ketterson, X. Liu, and R.P.H. Chang, “Large second harmonic response in ZnO thin films”, *Appl. Phys. Lett.* **80**, 401-403 (2002).

[24] X.Q. Zhang, Z.K. Tang, M. Kawasaki, A. Ohtomo, and H. Koinuma, ”Resonant exciton second-harmonic generation in self-assembled ZnO microcrystallites thin films”, *J. Phys. Condens.Matter* **15**, 5191-5196 (2003).

[25] X.Q. Zhang, Z.K. Tang, M. Kawasaki, A. Ohtomo, and H. Koinuma, “Second harmonic generation in self-assembled ZnO microcrystallite thin films”, *Thin Solid Films* **450**, 320-323 (2004).

[26] C.Y. Liu, B.P. Zhang, N.T. Binh, Y. Segawa, “Second harmonic generation in ZnO thin films fabricated by metalorganic chemical vapor deposition”, *Opt. Commun.* **237**, 65-70 (2004).

[27] M.C. Larciprete, D. Passeri, F. Michelotti, S. Paoloni, C. Sibilia, and M. Bertolotti, “Second order nonlinear optical properties of zinc oxide films deposited by low temperature dual ion beam sputtering”, *J. Appl. Phys.* **97**, 023501 (2005).

[28] M.C. Larciprete, D. Haertle, A. Belardini, M. Bertolotti, F.Sarto and P. Guenter, “Characterization of second and third order optical nonlinearities of ZnO sputtered films”, *Appl. Phys. B* **82**, 431-437 (2006).

[29] Ren-Chuan Chang, Sheng-Yuan Chu, Kuang-Yao Lo, Shih-Chieh Lo,and Yi-Ren Huang, “Physical and structural properties of RF magnetron sputtered ZnO films”, *Integrated Ferroelectrics* **69**, 43-53, (2005).

[30] B. Kulyk, Z. Essaidi, V. Kapustianyk, B. Turko, V. Rudyk, M. Partyka, M. Addou and B. Sahraoui, "Second and third order nonlinear optical properties of nanostructured ZnO, thin films deposited on a-BBO and $LiNbO_3$", *Optics Communications* **281**, 6107–6111 (2008).

[31] Kuang-Yao Lo, Shih-Chieh Lo, Chang-Feng Yu, Teddy Tite, Jung-Y. Huang, Yi-Jen Huang, Ren-Chuan Chang and Sheng-Yuan Chu, "Optical second harmonic generation from the twin boundary of ZnO thin films grown on silicon", *Appl. Phys. Lett.* **92**, 091909 (2008).

[32] Yi-Jen Huang, Kuang-Yao Lo, Chung-Wei Liu, Chun-Chu Liu, and Sheng-Yuan Chu, "Characterization of the quality of ZnO thin films using reflective second harmonic generation", *Appl. Phys. Lett.* **95**, 091904 (2009).

[33] U. Neumann, R. Grunwald, U. Griebner, G. Steinmeyer, M. Schmidbauer and W. Seeber, "Second-harmonic performance of *a*-axis-oriented ZnO nanolayers on sapphire substrates", *Appl. Phys. Lett.* **87**, 171108 (2005).

[34] G. Buinitskaya, L. Kulyuk, V. Mirovitskii, E. Rusu, E. Mishina, and N. Sherstyuk, "ZnO single crystal and epitaxial thin film studied by second harmonic generation and photoluminescence", *Superlattices and Microstructures* **39**, 83-90 (2006).

[35] J.S. Park, Y. Yamazaki, Y. Takahashi, S.K. Hong, J.H. Chang, T. Fujiwara and T. Yao, "Origin of second-order nonlinear optical response of polarity-controlled ZnO films", *Appl. Phys. Lett.* **94**, 231118 (2009).

[36] G.I. Petrov, V. Shcheslavskiy, V.V. Yakovlev, I. Ozerov, E. Chelnokov, and W. Marine, "Efficient third-harmonic generation in a thin nanocrystalline film of ZnO", *Appl. Phys. Lett.* **83**, 3993 (2003).

[37] C.Y. Liu, B.P. Zhang, N.T. Binh, Y. Segawa, "Third-harmonic generation from ZnO films deposited by MOCVD", Applied Physics B **79**, 83-86 (2004).

[38] L. Castañeda, O.G. Morales-Saavedra, D.R. Acosta, A. Maldonado and M. de la L. Olvera, "Structural, morphological, optical, and nonlinear optical properties of fluorine-doped zinc oxide thin

films deposited on glass substrates by the chemical spray technique", *Phys. Stat. Sol. (a)* **203**, 1971-1981 (2006).

[39] V. Narayanan, R.K. Thareja, "Harmonic generation in ZnO nanocrystalline laser deposited thin films", Optics Communications 260, 170-174 (2006).

[40] A. Zawadzka, P. Płóciennik, J. Strzelecki, B. Sahraoui , "Transparent amorphous zinc oxide thin films for NLO applications", Optical Materials **37,** 327-337 (2014).

[41] J. Khaled, T. Fujiwara, M. Ohama and A.J. Ikushima, "Generation of second harmonics in Ge-doped SiO_2 thin films by ultraviolet irradiation under poling electric field", *J. Appl. Phys.* **87**, 2137-2141 (2000).

[42] J. Yin, Z.G. Liu, H. Liu, X.S. Wang, T. Zhu and J.M. Liu, "The epitaxial growth of wurtzite ZnO fims on $LiNbO_3$ (0001) substrates", *J. Cryst. Growth **220***, 281-285(2000).

[43] N.A. Sanford and J.A. Aust, "Nonlinear optical characterization of $LiNbO_3$. I. Theoretical analysis of Maker fringe patterns for x-cut wafers", *J. Opt. Soc. Am. B.* **15**, 2885-2909 (1998).

[44] E.S. Tuzemen, S. Eker, H. Kavak and R. Esen, "Dependence of film thickness on the structural and optical properties of ZnO thin films", Applied Surface Science 255, 6195-6200 (2009).

[45] R.W. Terhune, P.D. Maker and C.M. Savage, "Optical Harmonic Generation in Calcite", *Phys. Rev. Lett.* **8**, 404-406 (1962).

[46] C.K. Chen, T.F. Heinz, D. Ricard and Y.R. Shen, "Detection of Molecular Monolayers by Optical Second-Harmonic Generation", *Phys. Rev. Lett.* **46**, 1010-1012 (1981).

[47] Y. Yan, M.M. Al-Jassim, M.F. Chisholm, L.A. Boatner, S.J. Pennycook and M. Oxley, "[1$\underline{1}$00]/(1102) twin boundaries in wurtzite ZnO and group-III-nitrides", *Phys. Rev. B* **71**, 041309 (2005).

[48] S.V. Andersen, V.Vandalon, R.H.E.C. Bosch, B.W.H. van de Loo, K. Pedersen and W.M.M. Kessels, "Interaction between O_2 and ZnO films probed by time-dependent second-harmonic generation", Appl. Phys. Lett. 104 , 051602 (2014).

[49] Ü. Özgür, Ya.I. Alivov, C. Liu, A. Teke, M.A. Reshchikov, S. Doan, V. Avrutin, S.-J. Cho, and H. Morkoç, "A comprehensive review of ZnO materials and devices", *J. Appl. Phys.* **98**, 041301 (2005).

[50] E.P. Zironi, J. Cañetas-Ortega, H. Gómez, A. Maldonado, R. Asomoza, and J. Palacios-Gomez, "Characterization of indium-doped zinc oxide films deposited by pyrolytic spray with different indium compounds as dopants", *Thin Solid Films* **293**, 117 (1997).

[51] M. Miki-Yoshida, F. Paraguay-Delgado, W. Estrada-Lopez and E. Andrade, "Structure and morphology of high quality indium-doped ZnO films obtained by spray pyrolysis", *Thin Solid Films* **376**, 99 (2000).

[52] M. de L. Olvera and A. Maldonado, "Characteristics of ZnO:Ga thin filmsprepared bychemical spray using two different Zn and Ga precursors", *Phys. Stat. Sol. (a)* **196**, 410 (2003).

[53] A. Ortiz, C. Falcony, J.A. Hernández, M. Garcia and J.C. Alonso, "Photoluminescent characteristics of lithium-doped zinc oxide films deposited by spray pyrolysis", *Thin Solid Films* **293**, 103-107 (1997).

[54] P.M.R. Kumar, C.S. Kartha, K.P. Vijayakumar, F. Singh and D.K. Avasthi, "Effect of fluorine doping on structural, electrical and optical properties of ZnO thin films", *Mater. Sci. Eng. B* **117,** 307-312(2005).

[55] F. Paraguay-Delgado, W. Estrada-Lopez, E. Andrade and M. Miki-Yoshida, "Influence of Al, In, Cu, Fe and Sn dopants in the microstructure of zinc oxide thin films obtained by spray pyrolysis", *Thin Solid Films* **366**, 16 (2000).

[56] O.G. Morales-Saavedra and L. Castañeda, "Second harmonic generation of fluorine-doped zinc oxide thin films grown on soda-lime glass substrates by a chemical spray technique", *Optics Communications* **269**, 370-377(2007).

[57] S.W. Liu, J.L. Weerasinghe, J. Liu, J. Weaver, C.L. Chen, W. Donner, and Min Xiao, "Reflective second harmonic generation near resonance in the epitaxial Al-doped ZnO thin film",*Optics Express* **15**, 10666-10671 (2007).

[58] F. Michelotti, R. Canali, L. Dominici, A. Belardini, F. Menchini, G. Schoer and J. Mueller, "Second order optical nonlinearity of ZnO/ZnO:Al bilayers deposited on glass by low temperature radiofrequency sputtering", *Appl. Phys. Lett.* **90**, 181110 (2007).

[59] C.C. Zheng, S.J. Xu, J.Q. Ning, Y.N. Chen, X.H. Lu, C.-C. Ling, C.M. Che, G.Y. Gao, J.H. Hao, G. Brauer and W. Anwand, "Ion-implantation induced nano distortion layer and its influence on nonlinear optical properties of ZnO single crystals", J. Appl. Phys. 110 , 083102 (2011).

[60] M. Abd-Lefdil, A. Belayachi, S. Pramodini, P. Poornesh, A.Wojciechowski and A. O. Fedorchuk, "Structural, photoinduced optical effects and third-order nonlinear optical studies on Mn doped and Mn–Al codoped ZnO thin films under continuous wave laser irradiation", Laser Phys. 24 035404 (2014).

[61] J.C. Johnson, H.Yan, R.D. Schaller, P.B. Petersen, P.Yang and R.J. Saykally, "Near-Field Imaging of Nonlinear Optical Mixing in Single Zinc Oxide Nanowires", Nano Letters 2 (4), 279-283 (2002).

[62] G. Wang, G. L. Wong and J. B. Ketterson, "Redetermination of second-order susceptibility of zinc oxide single crystals", Applied Optics 40, 5436-5438 (2001).

[63] S.W. Liu, H.J. Zhou, A. Ricca, R. Tian and M. Xiao, "Far field second-harmonic fingerprint of twinning in single ZnO rods", Phys.Rev.B 77, 113311 (2008).

[64] K. Geren, S.W. Liu, H.J. Zhou, Y. Zhang, R. Tian and Min Xiao, "Second-order susceptibilities of ZnO nanorods from forward second-harmonic scattering", J. Appl. Phys. 105, 063531 (2009).

[65] Chung-Wei Liu, Shoou-Jinn Chang, Chun-Chu Liu, Ruei-Jie Huang, Yan-Shen Lin, Min-Chia Su, Peng-Han Wang and Kuang-Yao Lo, "Inspecting the effects of post-annealing on ZnO nanorods by optical second harmonic generation", IEEE 5th International Nanoelectronics Conference (INEC), ISSN :2159-3523 E-ISBN:978-1-4673-4841-6, 505–507 (2013).

[66] Chung-Wei Liu, Shoou-Jinn Chang, Ching-Hung Hsiao, Ruei-Jie Huang, Yan-Shen Lin, Min-Chia Su, Peng-Han Wang, Kuang-Yao Lo, "Probing surface structure quality of ZnO nanorods by second harmonic generation", IEEE Photonics Technology Letters, 26, 789-792 (2014).

[67] S. Dhara, K. Imakita, M. Mizuhata and M. Fujii, “Europium doping induced symmetry deviation and its impact on the second harmonic generation of doped ZnO nanowires”, Nanotechnology 25, 225202 (2014).

[68] R. Prasanth, L.K. van Vugt, D.A.M. Vanmaekelbergh and H.C. Gerritsen, “Resonance enhancement of optical second harmonic generation in a ZnO nanowire”, Appl. Phys. Lett. 88, 181501 (2006).

[69] C.F. Zhang, Z.W. Dong, G.J. You, R.Y. Zhu, S.X. Qian, H. Deng, H. Cheng and J.C. Wang, “Femtosecond pulse excited two-photon photoluminescence and second harmonic generation in ZnO nanowires”, Applied Physics Letters 89, 042117 (2006).

[70] T. Voss, I. Kudyk, L. Wischmeier and J.Gutowski, “Nonlinear optics with ZnO nanowires”, Phys. Status Solidi B 246, No. 2, 311–314 (2009).

[71] K. Pedersen, C. Fisker and T.G. Pedersen, “Second-harmonic generation from ZnO nanowires”, Physica Status Solidi (C) Current Topics in Solid State Physics 5(8), 2671-2674 (2008).

[72] Jun Dai, Mao-Hui Yuan, Jian-Hua Zeng, Qiao-Feng Dai, Sheng Lan, Chai Xiao and Shao-Long Tie, “Controllable color display induced by excitation-intensity-dependent competition between second and third harmonic generation in ZnO nanorods”, Applied Optics 53, 189-194 (2014).

[73] Jun Dai, Jian-Hua Zeng, Sheng Lan, Xia Wan and Shao-Long Tie, “Competition between second harmonic generation and two- photon induced luminescende in single, double and multiple ZnO nanorods”, Optics Express 21, 10025- 10038 (2013).

[74] Jun Dai, Qiao-Feng Dai, Jian-Hua Zeng, Sheng Lan, Xia Wan and Shao-Long Tie, “Negative slope for second harmonic generation observed at high excitation intensities in ZnO nanorods”, IEEE Journal of Quantum Electronics 49, 903-909 (2013).

[75] Weiwei Liu, Kai Wang, Hua Long, Sheng Chu, Bing Wang and Peixiang Lu, “Near-resonant second-order nonlinear susceptibility in c-axis oriented ZnO nanorods”, Appl. Phys. Lett. 105 , 071906 (2014); http://dx.doi.org/10.1063/1.4893599.

[76] S.W. Chan, R. Barille, J.M. Nunzi, K.H. Tam, Y.H. Leung, W.K. Chan, A.B. Djurisi˘c´, “Second harmonic generation in zinc oxide nanorods”, Appl. Phys. B 84, 351-355 (2006).

[77] S. Kumar Das, M. Bock, C. O'Neill, R. Grunwald, K. Moon Lee, H. Woon Lee, S. Lee and F. Rotermund, “Efficient second harmonic generation in ZnO nanorod arrays with broadband ultrashort pulses”, Applied Physics Letters 93, 181112 (2008).

[78] Guan-Yu Zhuo, Kuo-Jen Hsu, Tung-Yu Su, Nan-Hsun Huang, Yang-Fang Chen and Shi-Wei Chu, “Effect of Lorentz local field for optical second order nonlinear susceptibility in ZnO nanorod”, J. Appl. Phys. 111 , 103112 (2012).

[79] Ying Wang, “Local field effect in small semiconductor clusters and particles”, J. Phys. Chem. 95 (3), 1119-1124 (1991).

[80] X. Lu, H. Zhou, G.J. Salamo, Z. Ryan Tian and M. Xiao, “Generation of exciton-polaritons in ZnO microcrystallines using second-harmonic generation”, New J. Phys. 14, 073017, (2012).

[81] A. Chaieb, A. Chari and B. Sahraoui, “Optical properties of ZnO nanocrystals embedded in PMMA”, Opt. Quant. Electron 46, 39-46 (2014).

[82] B.E. Urban, P. Neogi, K. Senthilkumar, S.K. Rajpurohit, P. Jagadeeshwaran, S. Kim, Y. Fujita and A. Neogi, “Bioimaging using the optimized nonlinear optical properties of ZnO nanoparticles”, IEEE Journal on Selected Topics in Quantum Electronics 18(4), 1451-1456 (2012).

[83] R. Le Dantec, Y. Mugnier, G. Djanta, L. Bonacina, J. Extermann, L. Badie, C. Joulaud and M. Gerrmann, “Ensemble and Individual Characterization of the Nonlinear Optical Properties of ZnO and BaTiO3 Nanocrystals”, Journal of Physical Chemistry C. 115(31), 15140-15146 (2011).

[84] S.L. Shi, S.J. Xu, Z.X. Xu, V.A. L. Roy and C.-M. Che, “Broadband second harmonic generation from ZnO nano-tetrapods”, Chemical Physics Letters 506, 226-229 (2011).

[85] C.C. Zheng, S.J. Ku, J.Q. Ning, S.F. Zhang, J.Y. Wang, C.M. Che and J.H. Hao, “Inner surface enhanced femtosecond second harmonic generation in thin ZnO crystal tubes”, Journal of Applied Physics 109, 013528 (2011).

[86] J.I. Jang, S. Park, N.L. Frazer, J.B. Ketterson, S. Lee, B.K. Roy and J. Cho, “Strong P-band emission and third harmonic generation from ZnO nanorods”, Solid State Communications 152, 1241–1243 (2012).

[87] H.W. Lee, K.M. Lee, S. Lee, K.H. Koh, J.-Y. Park, K. Kim and F. Rotermund, “Ultrafast third-order optical nonlinearities of vertically-aligned ZnO nanorods”, Chemical Physics Letters 447, 86-90 (2007).

[88] B. Kulyk, Z. Essaidi, J. Luc, Z. Sofiani, G. Boudebs, B. Sahraoui, V. Kapustianyk and B. Turko, “Second and third order nonlinear optical properties of microrod ZnO films deposited on sapphire substrates by thermal oxidation of metallic zinc”, Journal of Applied Physics 102, 113113 (2007).

[89] S.K. Das, F. Güell and C. Gray, “ZnO nanorods for efficient third harmonic UV generation”, Optical Materials Express 4 , 701-709 (2014).

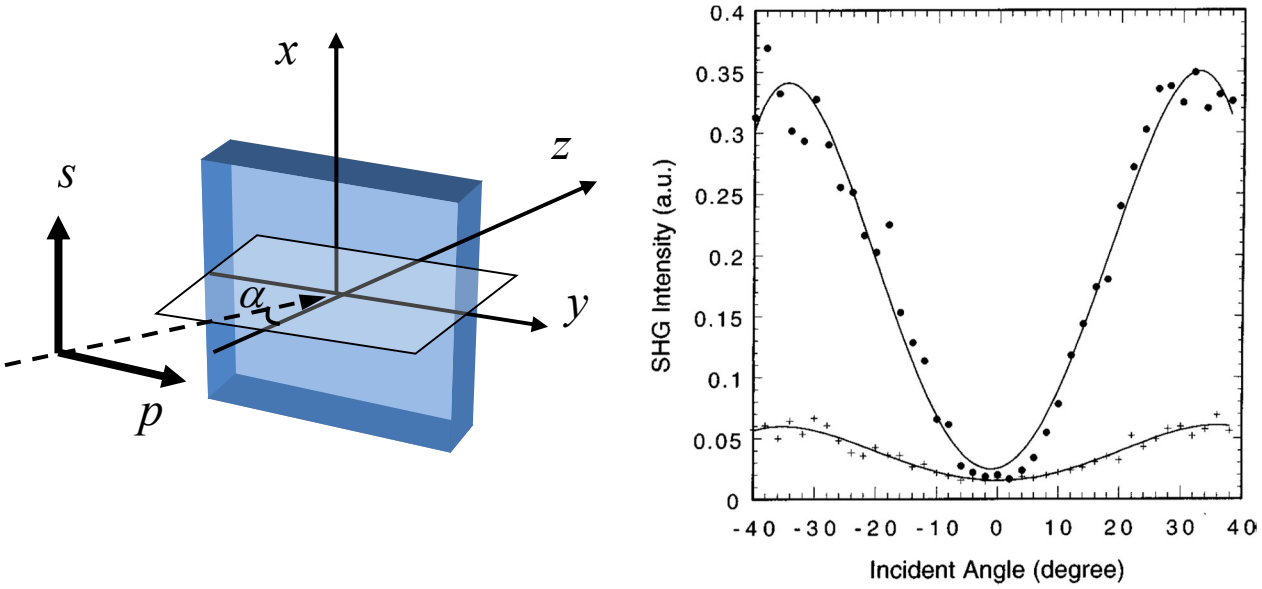

Figure 1. (a) Sketch of the sample in the Maker fringes experimental configuration. Thick arrows identify two different polarization state for the incident beam.(b) Measured SHG intensities from a ZnO film, 45 nm thick, as a function of the incident angle of the fundamental beam, when the fundamental beam is p-polarized (closed circles) and s-polarized (crosses). The solid curves correspond to theoretical fitting. Reprinted with permission from H. Cao, J. Y. Wu, H. C. Ong, J. Y. Dai, and R. P. H. Change, Applied Physics Letters, Vol.73, Page 573, (1998). Copyright 1998, American Institute of Physics.

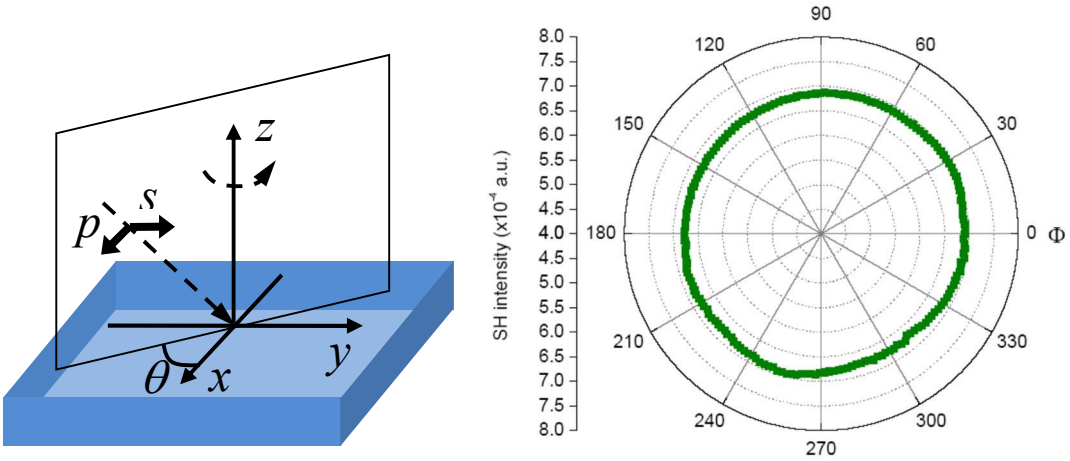

Figure 2. (a) Sketch of the RSHG experimental configuration. Thick arrows identify the different polarization state for the incident beam. (b) Reflective second harmonic generation (RSHG) pattern arising from Al-doped ZnO thin film, about 285 nm thick. Both fundamental and generated beams are p-polarized (from [52]). Reprinted from S. W. Liu, J. L. Weerasinghe, J. Liu, J. Weaver, C.L. Chen, W. Donner, and Min Xiao, "Reflective second harmonic generation near resonance in the epitaxial Al-doped ZnO thin film", Optics Express 15, 10666-10671 (2007).

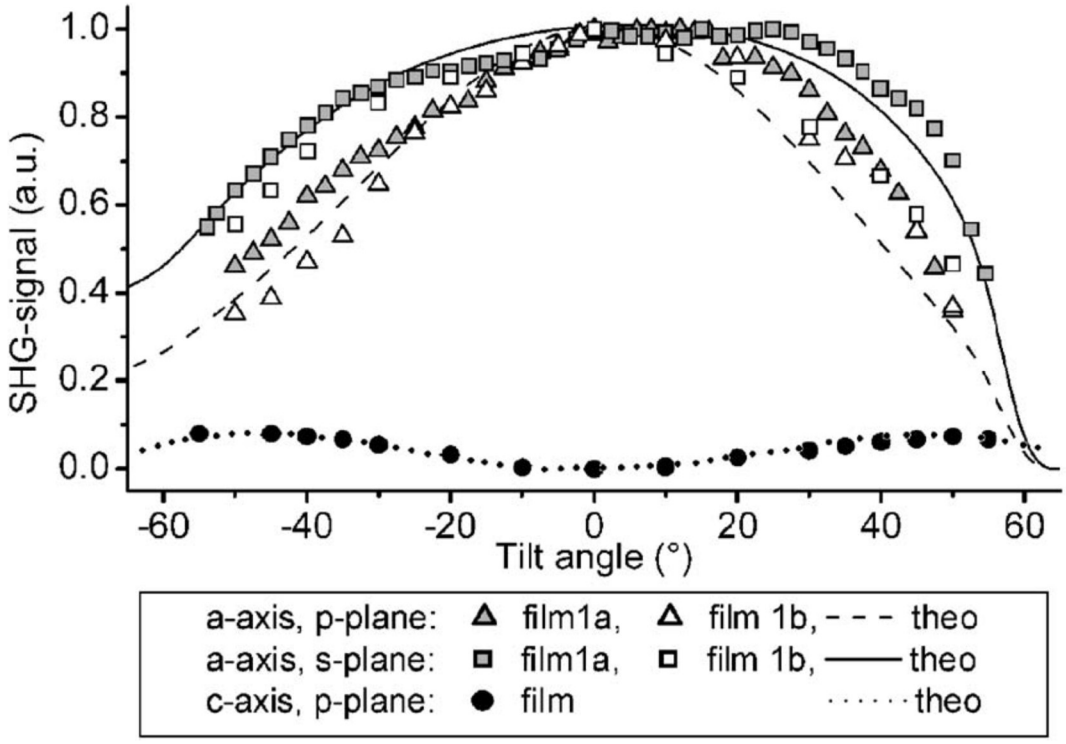

Figure 3. Measured (symbols) and simulated (lines) dependence of the SHG intensity on incidence angle. The asymmetry stems from saw-tooth like facetting of the crystallites. Both, a-axis and c-axis oriented ZnO films have been considered for tilt in the p- and the s-polarization plane. Theoretical curves are based on identical $\chi^{(2)}$ tensor values, assuming a 6° tilt angle of the crystallite facettes relative to the surface. Film1a and film1b refer to the two different samples [28]. The c-axis values are shown for comparison. Reprinted with permission from U. Neumann, R. Grunwald, U. Griebner, G. Steinmeyer, M. Schmidbauer, and W. Seeber, "Second-harmonic performance of a-axis-oriented ZnO nanolayers on sapphire substrates", Appl. Phys. Lett. ***87****, 171108 (2005). Copyright 2005, American Institute of Physics.*

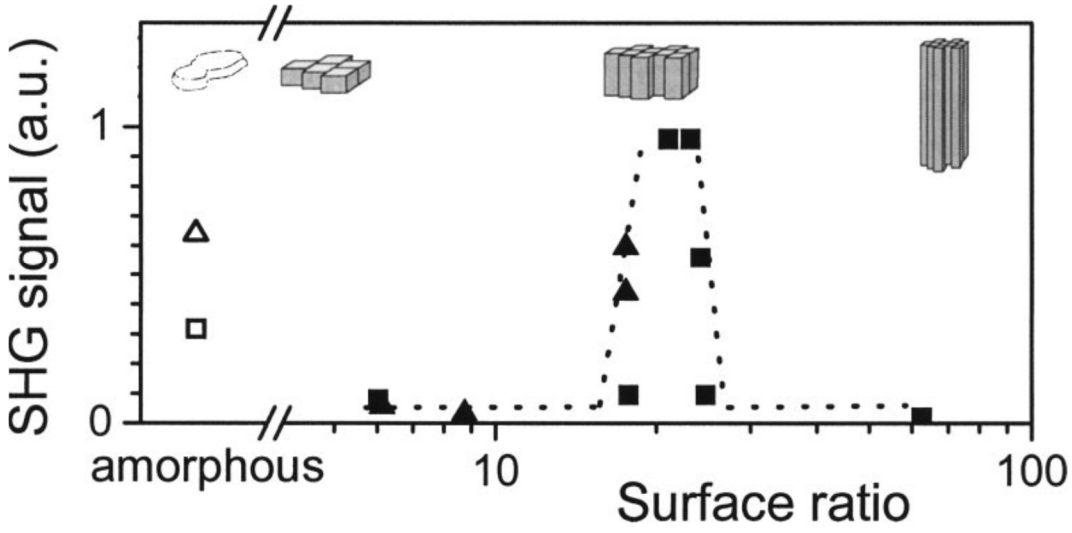

Figure 4. Relative strength of SHG signals vs. surface ratio, σ. The dashed line was included to guide the eye. Crystallite aspect ratios are visualized for the range measured. Reprinted with permission from U. Neumann, R. Grunwaid, U. Griebner, G. Steinmeyer, W. Seeber, Applied Physics Letters, Vol.84, Page 171, (2004). Copyright 2004, American Institute of Physics.

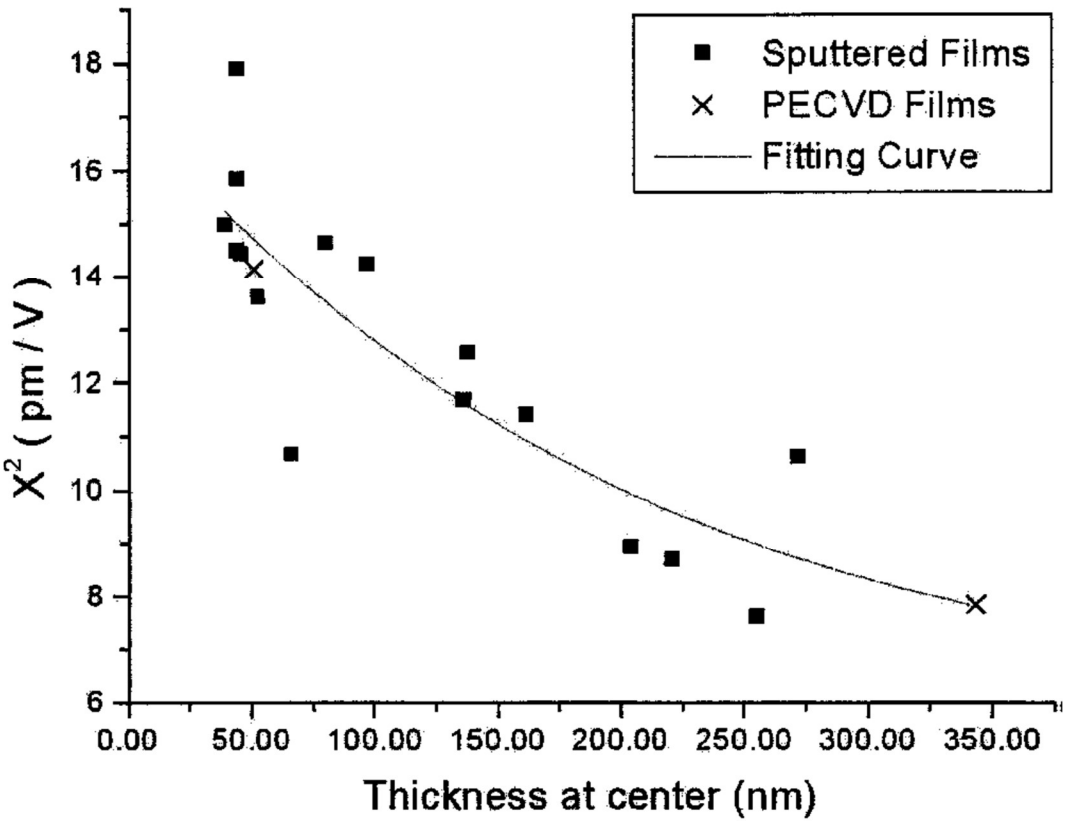

Figure 5. Film thickness dependence of the larger component of the susceptibility, $\chi_{33}^{(2)}$ (from [18]). Reprinted with permission from G. Wang, G.T. Kiehne, G.K. Wong, J.B. Ketterson, X. Liu, R.P.H. Chang, Applied Physics Letters, Vol.80, Page 402, (2002). Copyright 2002, American Institute of Physics.

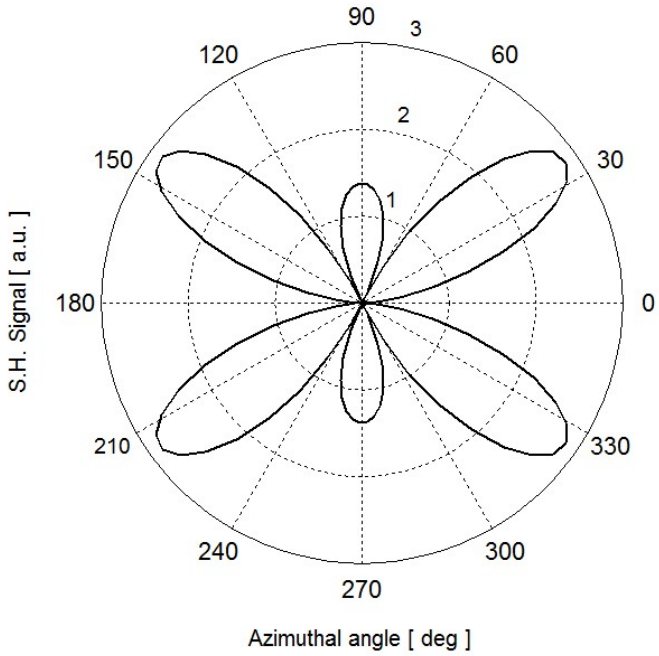

Figure 6. Theoretical simulation of RSHG patterns for both fundamental and generated beams s-polarized, calculated via Equation (9). The typical six-fold pattern reflects the contribute of both polar surface and twin boundaries.

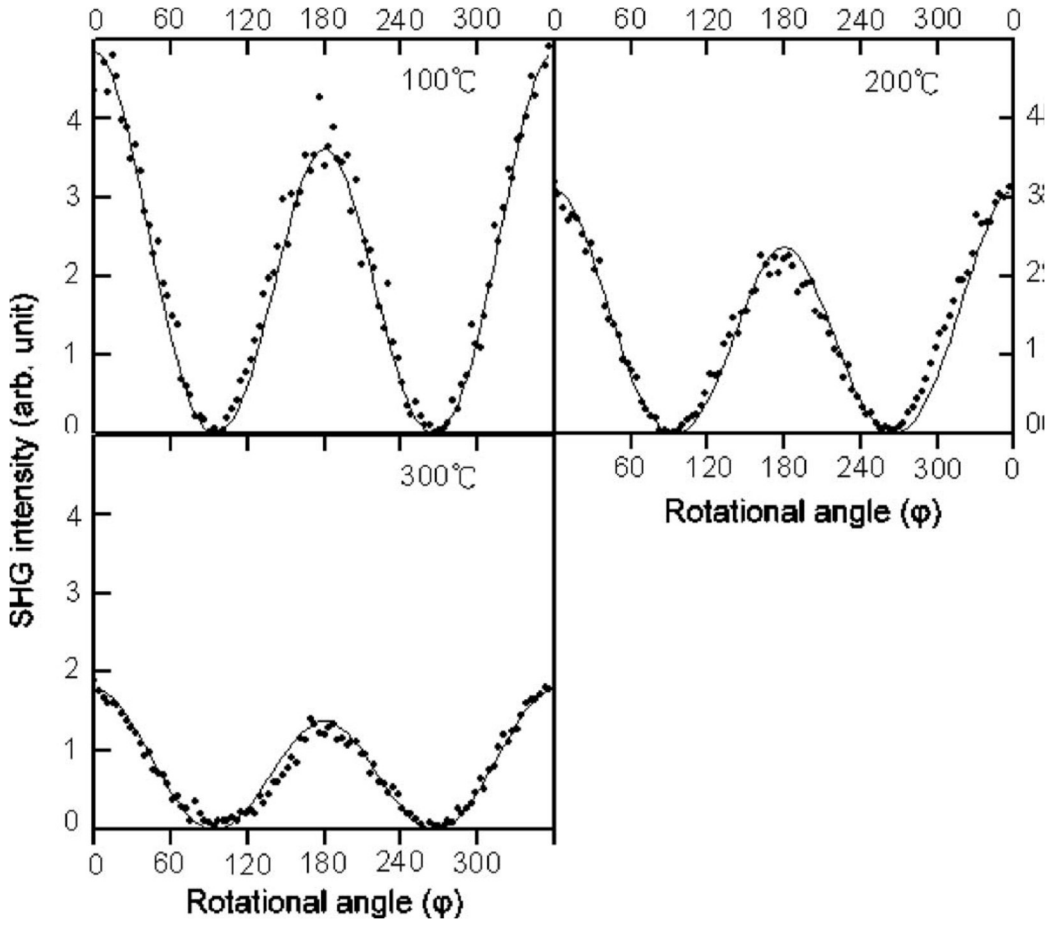

Figure 7. The RSHG pattern measured from a ZnO film on Si (111) substrate deposited at a temperature of 100, 200 and 300 °C respectively. Both fundamental and generated beams are s-polarized (from [22]). Reprinted with permission from Kuang-Yao Lo, Shih-Chieh Lo, Chang-Feng Yu, Teddy Tite, Jung-Y. Huang, Yi-Jen Huang, Ren-Chuan Chang, and Sheng-Yuan Chu, Applied Physics Letters, Vol.92, Page 091909-2, (2008). Copyright 2008, American Institute of Physics.

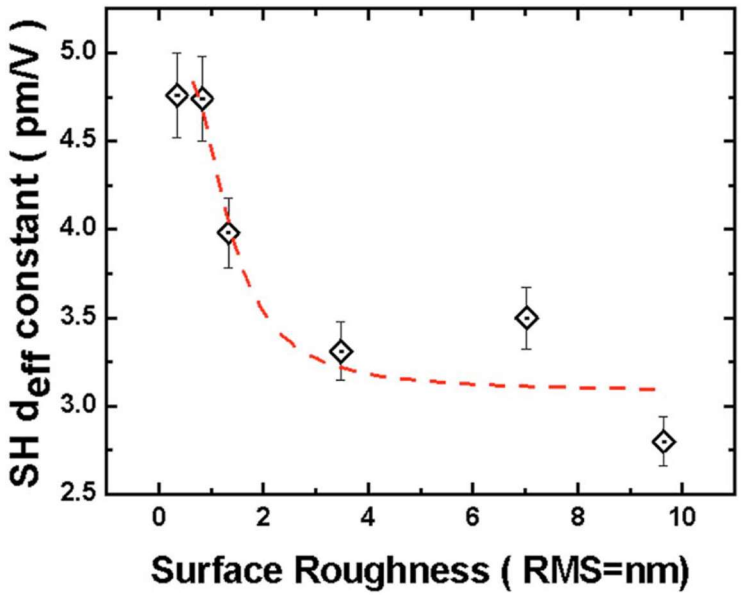

Figure 8. The effective second-order nonlinear coefficient as a function of surface roughness addressed by RMS. The dotted line shows the Lorentzian fitting curves (from [26]). Reprinted with permission from J. S. Park, Y. Yamazaki, Y. Takahashi, S. K. Hong, J. H. Chang, T. Fujiwara, and T. Yao, Applied Physics Letters, Vol.94, Page 231118-3, (2009). Copyright 2009, American Institute of Physics.

(a)

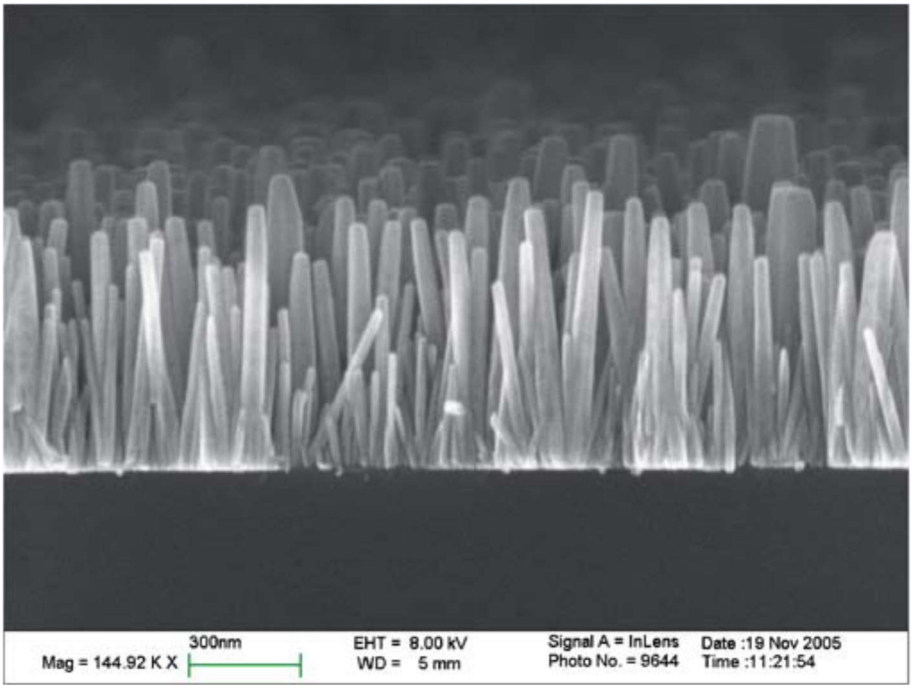
300nm
Mag = 144.92 K X
EHT = 8.00 kV
WD = 5 mm
Signal A = InLens
Photo No. = 9644
Date :19 Nov 2005
Time :11:21:54

(b)

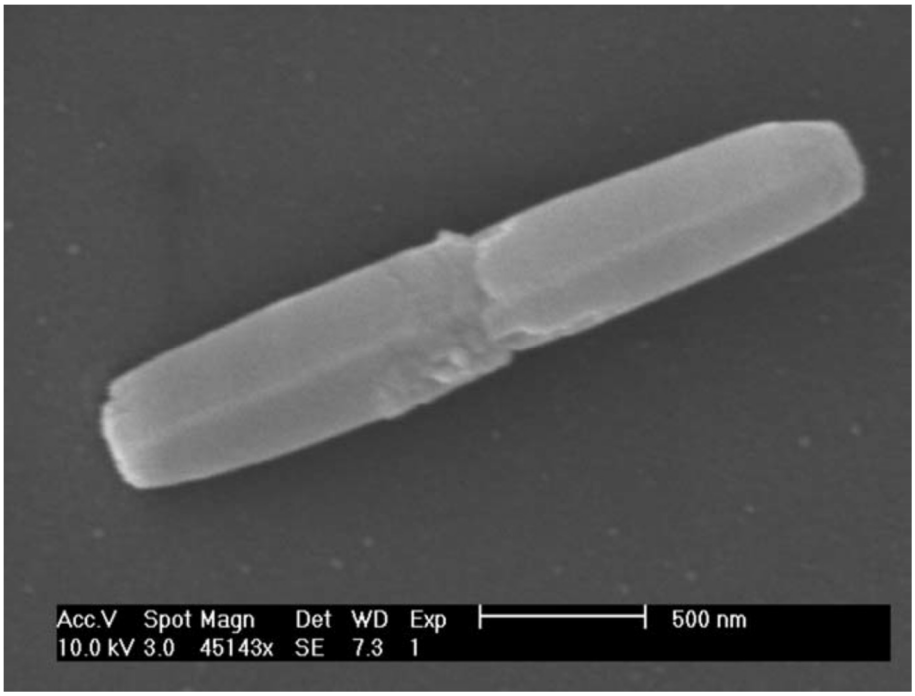
Acc.V Spot Magn Det WD Exp
10.0 kV 3.0 45143x SE 7.3 1
500 nm

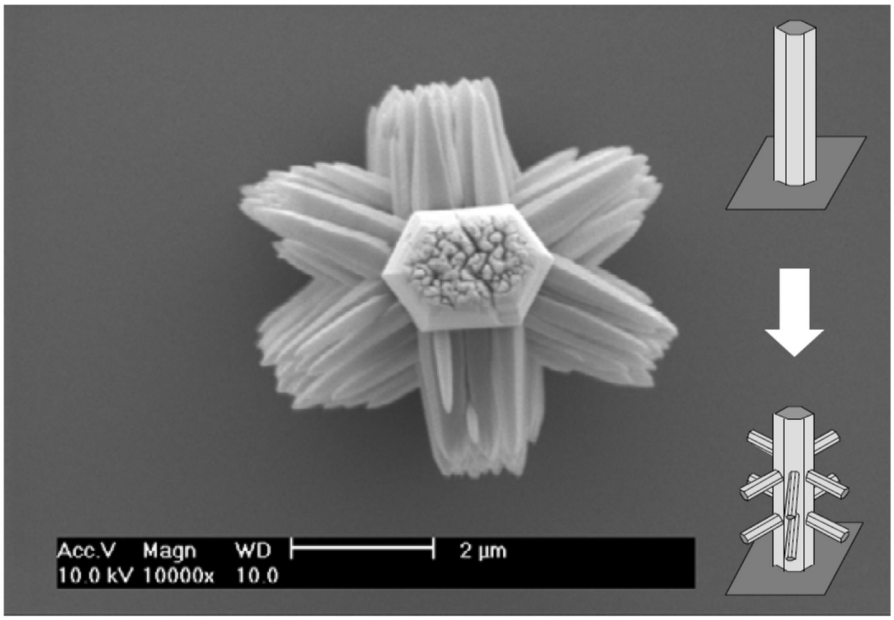

(c)

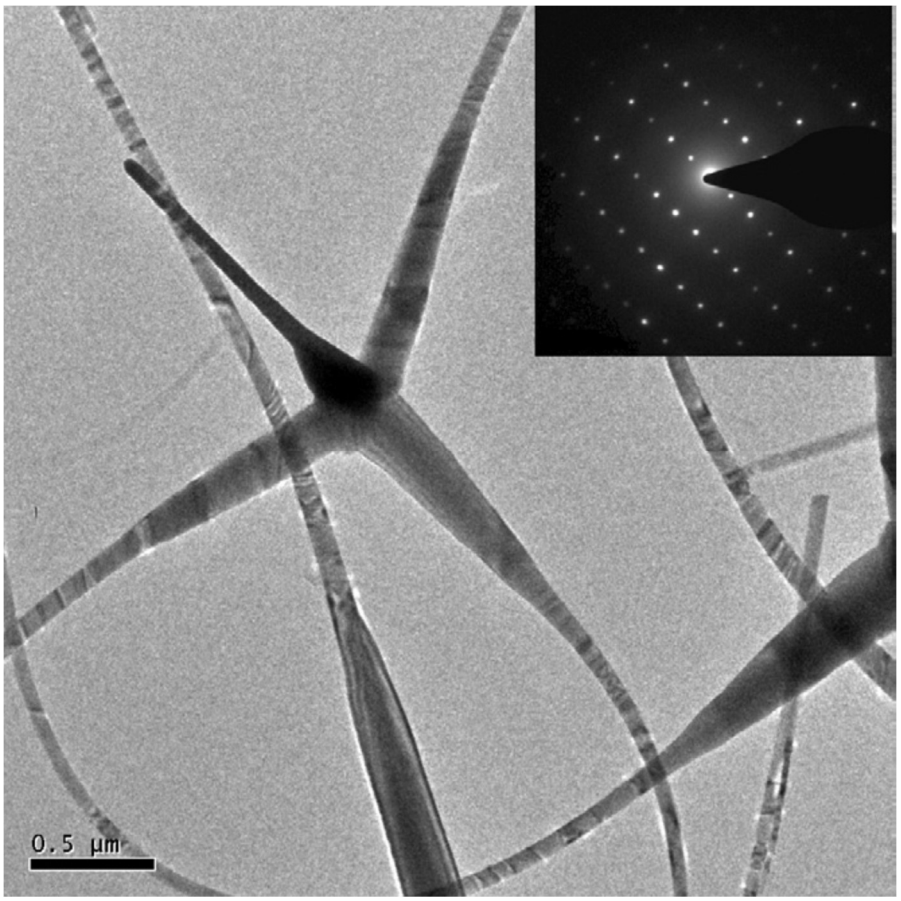

(d)

Figure 9.

(a) Side-view SEM image of ZnO nanorod samples grown for 7.5 h onto glass substrate by an aqueous solution method.

S.W.Chan, R. Barille, J.M. Nunzi, K.H. Tam, Y.H. Leung, W.K. Chan, A.B. Djurisi˘c´, "Second harmonic generation in zinc oxide nanorods", Appl. Phys. B 84, 351-355 (2006).

(b) SEM image of a ZnO rod with the twinned structure, the twinning interface at the centre.

S.W.Liu, H.J.Zhou, A.Ricca, R.Tian and M.Xiao, "Far field second-harmonic fingerprint of twinning in single ZnO rods", Phys.Rev.B 77, 113311 (2008).

(c) A SEM image of a tree-like ZnO microcrystalline showing branches of nanowires with lateral size in the range of 50-400nm and length of about 2-3 microns.

X Lu, Huajun Zhou, G J Salamo, Z Ryan Tian, and Min Xiao, "Generation of exciton-polaritons in ZnO microcrystallines using second-harmonic generation", New J. Phys. 14 073017, (2012).

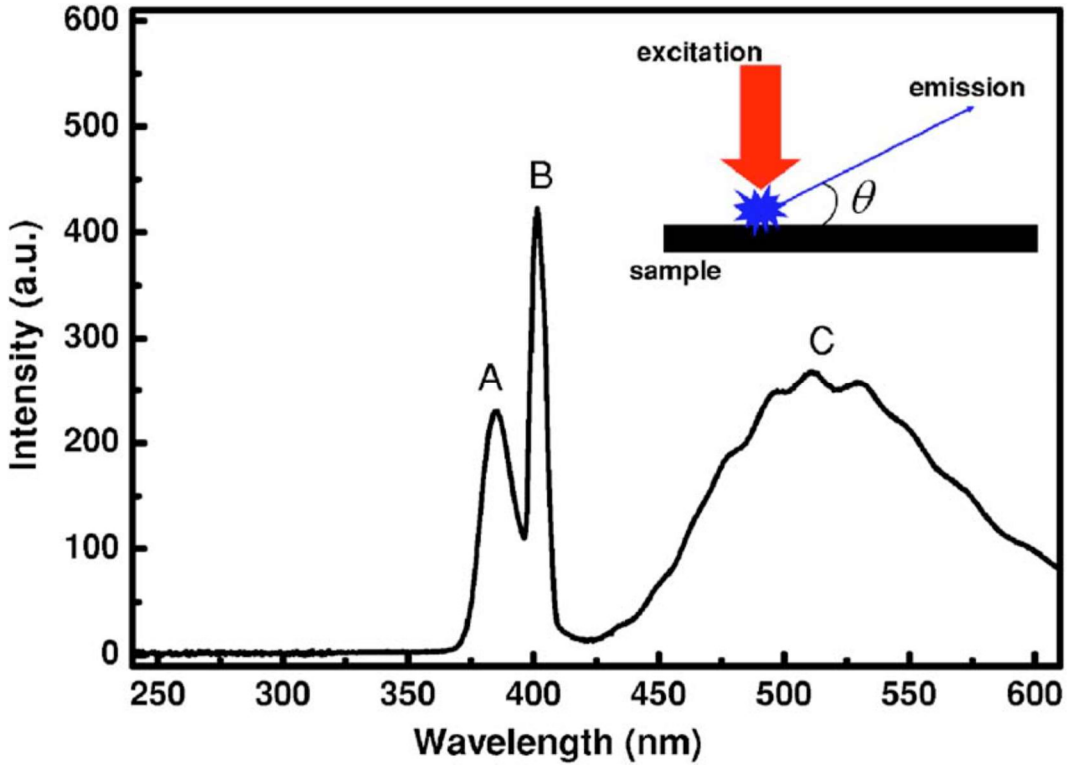

Figure 10. PL emission spectrum as a function of wavelength of ZnO nanowires excited with 806 nm and measured with a tilt angle θ of 30°. Reprinted with permission from C. F. Zhang, Z. W. Dong, G. J. You, R. Y. Zhu, S. X. Qian, H. Deng, H. Cheng, and J. C. Wang, "Femtosecond pulse excited two-photon photoluminescence and second harmonic generation in ZnO nanowires", Applied Physics Letters 89, 042117 (2006). Copyright 2006, American Institute of Physics.

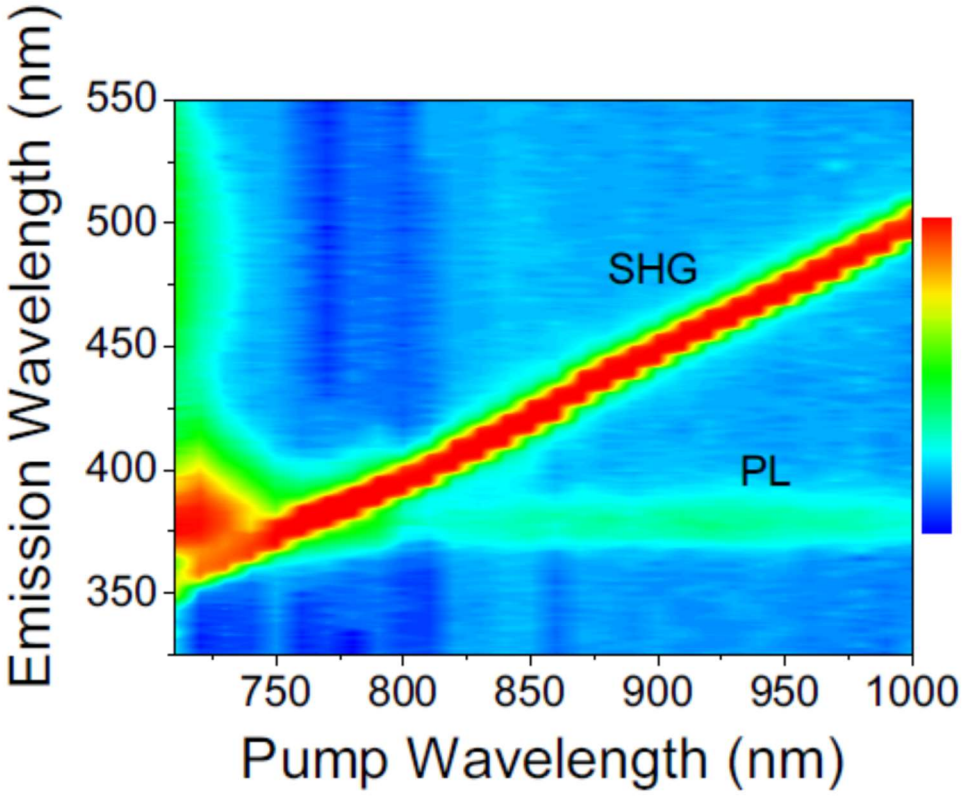

Figure 11 Contour plot showing light emission intensity as a function of pump emission wavelength.. Stuctures due to SHG and multi-photon photoluminescence are marked.

Pedersen, K. , Fisker, C., Pedersen, T.G. , "Second-harmonic generation from ZnO nanowires", Physica Status Solidi (C) Current Topics in Solid State Physics, Volume 5, Issue 8, Pages 2671-2674 (2008).

Table I. SHG in ZnO thin films.

Deposition Technique	Substrate	Laser Source	Thickness	d_{ij} Value	Reference
Dual ion beam sputtering.	Glass.	λ=1064 nm τ_{pulse}=5 ns f_{rep}=14 Hz	370 nm	$\lvert d_{33} \rvert$= 1.23 pm/V	[22]
Dual ion beam sputtering.	Glass.	λ=1064 nm τ_{pulse}=7 ns f_{rep}=14 Hz	550 nm	d_{33}= 0.90 pm/V d_{15}= 0.53 pm/V d_{31}= 0.31 pm/V	[23]
		λ=1542 nm τ_{pulse}=7 ns f_{rep}=14 Hz		d_{33}= 0.25 pm/V d_{15}= 0.14 pm/V d_{31}= 0.10 pm/V	
		λ=1907 nm τ_{pulse}=7 ns f_{rep}=14 Hz		d_{33}= 0.16 pm/V d_{15}= 0.08 pm/V d_{31}= 0.08 pm/V	
Metal organic aerosol deposition.	Sapphire	λ=790 nm τ_{pulse}=35 fs f_{rep}=1 kHz	150 nm	d_{33}= -12 pm/V d_{31}= d_{32}= 2.8 pm/V	[28] *a*-axis oriented films.
			300 nm	d_{33} = -15 pm/V d_{31}= d_{32}= 4.9 pm/V	
ZnO single crystal platelets.	(0001) orientation.	1064 nm		d_{33}= -7.15 pm/V d_{31}= 0.68 pm/V	[57]
	(10$\underline{1}$0) orientation.			d_{33}= -7.38 pm/V d_{31}= 0.70 pm/V	

Table II.

Deposition Technique	Substrate	Laser Source	Thickness	d_{ij} Value	Reference
Pulsed laser ablation.	Sapphire.	λ=1064 nm τ_{pulse}=5 ns f_{rep}=10 Hz	45 nm	Highly crystalline film d_{33} =5.4 pm/V d_{31} =1 pm/V	[14]
			45 nm	Low crystalline film d_{33} =6.7 pm/V d_{31} =1.8 pm/V	
			235 nm	Hihghly crystalline film d_{33} =2.05 pm/V d_{31} =0.5 pm/V	
			235 nm	Low crystalline film d_{33} =4.4 pm/V d_{31}=0.7 pm/V	
Spray pyrolysis.	Glass.	λ=830 nm τ_{pulse}=20 fs f_{rep}=88 MHz	0.1–1.0 micron	d_{31}= d_{32}=2.1 pm/V d_{15}= d_{24}=2.6 pm/V d_{33}= -7.3 pm/V	[16]
MOCVD	Sapphire.	λ=1064 nm τ_{pulse}=7 ns f_{rep}=10 Hz	350 nm	Deposited at 200 °C d_{33}= 3.60 pm/V d_{31}= 1.12 pm/V	[21]
			350 nm	Deposited at 250 °C d_{33}= 4.60 pm/V d_{31}= 1.62 pm/V	

			350 nm	Deposited at 300 °C d_{33}= 1.60 pm/V d_{31}= 0.47 pm/V	
Rf magnetron sputtering.	α-BBO substrate	λ=1064 nm τ_{pulse}=16 ps f_{rep}=10 Hz	1.2 micron	$d_{eff}^{(2)}$ =0.11 pm/V	[25]
	$LiNbO_3$ substrate		1.2 micron	$d_{eff}^{(2)}$ =6.45 pm/V	
Plasma assisted deposition.	Fused silica	λ=1064 nm τ_{pulse}=8 ms f_{rep}=10 Hz		Deposited at 100 mTorr $\chi^{(2)}_{eff}$= 3.2 pm/V	[34]
				Deposited at 900 mTorr $\chi^{(2)}_{eff}$ = 0.7 pm/V	

Table III.

Deposition Technique	Substrate	Laser Source	Thickness	d_{ij} Value	Reference
Plasma-enhanced CVD.	Sapphire	λ=1064 nm	44.2 nm	d_{33} = 8.94 pm/V	[18]
	Sapphire		343.5 nm	d_{33}= 3.90 pm/V	
Laser molecular beam epitaxy.	Sapphire.	λ=720-1100 nm τ_{pulse}=35 ps f_{rep}=10 Hz	44.4 nm	d_{33}= -83.7 pm/V d_{15}= 15.2 pm/V d_{31}= 14.7pm/V	[20]

Table IV.

Deposition Technique	Substrate	Laser Source	Thickness	d_{ij} Value	Reference
Chemical spray technique.	Glass.	λ=1064 nm τ_{pulse}=5 ns f_{rep}=25 kHz	570 nm	d_{33}= 13.2 pm/V d_{31}= 5.15 pm/V	[33] F doping
Chemical spray deposition.	Glass.	λ=1064 nm τ_{pulse}=5 ns f_{rep}=12 kHz	540 nm	d_{33}= 8.20 pm/V d_{31}= 2.65 pm/V	[51] F doping
Commercial	Sapphire.	λ=810 nm τ_{pulse}=300 fs f_{rep}=82 MHz	285 nm	d_{33}= 3.27 pm/V d_{15}= 0.35 pm/V d_{31}= 0.13 pm/V	[52] Al doping

Table V. SHG from ZnO nanowires and nanorods.

Deposition Technique	Substrate	Laser Source	Diameter, ⦰ Length, L	d_{ij} Value	Reference
Sonication and dispersion	Sapphire	λ=800 nm τ_{pulse}= 800 fs f_{rep}= 1 kHz	⦰ 80-100 nm	$\chi^{(2)}_{31}$ = 2.5 pm/V $\chi^{(2)}_{33}$ = 5.5 pm/V	[56]
Aqueous solution method		λ= 810 nm τ_{pulse}=100 fs	⦰ 100-250 nm L Some μm	d_{33}= -3 pm/V d_{31}= 0.56 pm/V d_{15}=0.86 pm/V	[64]
Aqueous solution method	ZnO-seeded glass	λ=1044 nm τ_{pulse}=280 fs	⦰ 100 nm L 1 μm	d_{33}=0.4 pm/V *before annealing* d_{33} =0.65 pm/V *after annealing*	[60]
Modified aqueous chemical growth method	Quartz substrate	λ=800 nm τ_{pulse}=70 fs f_{rep}= 82 MHz	⦰70-100 nm L few μm	d_{eff} 12.57 pm/V undoped wires highest d_{eff} =19.09 pm/V for 1% Eu doping	[62]
CVD method	Si substrate	λ=800 nm τ_{pulse}= 50 fs f_{rep}= 80 MHz	⦰100-500 nm	d_{15} = 10.2 pm/V	[70]
Aqueous solution method	Glass		L/⦰=5.7 L/⦰=10.8	d_{31} = 0.14 pm/V d_{33} = -7.8 pm/V d_{31} = 2.88 pm/V	[71]

				d_{33} = -18.0 pm/V	
Low temperature chemical bath method	Glass	λ= 806 nm τ_{pulse}=13 fs	⦰ 56 nm L 1.3 μm ⦰ 59 nm L 0.87μm ⦰ 95 nm L 1.02 μm	d_{eff}=15 pm/V d_{eff}=2pm/V d_{eff}= 3.2 pm/V	[72]
Hydrothermal method	Indium tin oxide (ITO) glass plate	λ= 1034 nm τ_{pulse}=430 fs	⦰60 L 0.36 μm ⦰280 L 3.7 μm	$\chi^{(2)}_{31}$ = 0.59 pm/V $\chi^{(2)}_{33}$ = -2.77 pm/V $\chi^{(2)}_{31}$ = 1.98 pm/V $\chi^{(2)}_{33}$ = -19.06 pm/V)	[73]
Colloidal solution and then spin coating	Matrix of polymethylmeth acrylate	λ= 1064 nm τ_{pulse}=16 ps	nanocrystals with very small radius (1.8 nm)	d_{33}= 297.5 pm/V d_{31}= -148.5 pm/V	[76]
ZnO nanopowders, dispersed into water or ethanol. 20 nm and ZnO 200 nm		λ= 1064 nm τ_{pulse}=1 ns	⦰ 20 nm ⦰ 200 nm,	(d_{xxx}= 0.7-1.8 pm/V) (d_{xxx}=1.1-2 pm/V)	[78]

Table VI. Third harmonic generation from ZnO films and nanostructures.

Deposition Technique	Substrate	Laser Source	Thickness	$\chi^{(3)}$ Value	Reference
Dual ion beam sputtering	Glass	1907 nm	500 nm	$\chi^{(3)}_{3333} = 1.32 \cdot 10^{-12}$ esu = $1.85 \cdot 10^{-20}$ m^2/V^2	[23]
Pulsed laser ablation	Fused silica	1250 nm	1 μm	$\chi^{(3)} = 1.4 \times 10^{-12}$ esu	[31]
MOCVD				$\chi^{(3)} = 3.77 \cdot 10^{-12}$ Esu	[37]
chemical spray technique	sodacalcic glass	1064 nm	500 nm	$\chi^{(3)}_{ZnO:F} = 0.72 \cdot 10^{-12}$ esu = $1.0 \cdot 10^{-20}$ (m^2/V^2)	[33]
Laser deposited				$\chi^{(3)} =$ $9.56 \cdot 10^{-12}$ esu (8nm) $1.2 \cdot 10^{-13}$ esu (84nm)	[39]
Dip-coating (sol-gel) method		1064 nm		$\chi^{(3)}_p = 1.68 \cdot 10^{-18}$ m^2/V^2 $\chi^{(3)}_s = 1.60 \cdot 10^{-18}$ m^2/V^2 $\chi^{(3)}_p = 7.20 \cdot 10^{-18}$ m^2/V^2 $\chi^{(3)}_s = 6.68 \cdot 10^{-18}$ m^2/V^2	[40]
Thermal oxidation of metallic Zn		1064nm 16ps	3-4 μm	$\chi^{(3)}_{eff} = 71$ and $60 \cdot 10^{-22}$ m^2/V^2,	[83]